



Review

Merged Tacrine-Based, Multitarget-Directed Acetylcholinesterase Inhibitors 2015–Present: Synthesis and Biological Activity

Todd J. Eckroat * , Danielle L. Manross and Seth C. Cowan

School of Science, Penn State Erie, The Behrend College, Erie, PA 16563, USA; dmm6518@psu.edu (D.L.M.); svc5855@psu.edu (S.C.C.)

* Correspondence: tje146@psu.edu; Tel.: +1-814-898-6839

Received: 30 June 2020; Accepted: 17 August 2020; Published: 19 August 2020



Abstract: Acetylcholinesterase is an important biochemical enzyme in that it controls acetylcholine-mediated neuronal transmission in the central nervous system, contains a unique structure with two binding sites connected by a gorge region, and it has historically been the main pharmacological target for treatment of Alzheimer’s disease. Given the large projected increase in Alzheimer’s disease cases in the coming decades and its complex, multifactorial nature, new drugs that target multiple aspects of the disease at once are needed. Tacrine, the first acetylcholinesterase inhibitor used clinically but withdrawn due to hepatotoxicity concerns, remains an important starting point in research for the development of multitarget-directed acetylcholinesterase inhibitors. This review highlights tacrine-based, multitarget-directed acetylcholinesterase inhibitors published in the literature since 2015 with a specific focus on merged compounds (i.e., compounds where tacrine and a second pharmacophore show significant overlap in structure). The synthesis of these compounds from readily available starting materials is discussed, along with acetylcholinesterase inhibition data, relative to tacrine, and structure activity relationships. Where applicable, molecular modeling, to elucidate key enzyme-inhibitor interactions, and secondary biological activity is highlighted. Of the numerous compounds identified, there is a subset with promising preliminary screening results, which should inspire further development and future research in this field.

Keywords: acetylcholinesterase; tacrine; Alzheimer’s disease; multitarget-directed ligand; pyranopyrazole; Friedländer reaction

1. Introduction

Acetylcholinesterase (AChE; EC 3.1.1.7) catalyzes the hydrolysis reaction of acetylcholine (ACh) to choline and acetate (Figure 1A), making it responsible for terminating ACh-mediated synaptic transmission in the central nervous system (CNS) with high catalytic efficiency [1,2]. Structurally, three key features are known: The catalytic active site (CAS), the gorge, and the peripheral anionic site (PAS) (Figure 1B,C). The CAS is in the interior of the enzyme and is where the hydrolysis reaction takes place. It can be further divided into regions including the esteratic site, which contains the catalytic triad (Ser203, His447, Glu334 in *hAChE* (PDB:4EY4)), the anionic site, which contains aromatic residues (Trp86, Tyr133, Tyr337, Phe338) that stabilize the quaternary ammonium group of ACh through cation- π interactions, the oxyanion hole, which contains residues (Gly121, Gly122, Ala204) to stabilize the negatively charged transition state, and the acyl pocket, which uses residues (Phe295 and Phe297) to control substrate specificity. The gorge region, having dimensions of about 20 Å long and 5 Å wide, connects the CAS to the PAS and the enzyme exterior. It is lined with primarily aromatic amino acids. The PAS on the exterior of the enzyme also consists of primarily aromatic residues (Tyr72,

Asp74, Tyr124, Trp286, Tyr341) and serves as a low affinity binding site to concentrate ACh at the entrance to the gorge [3–9].

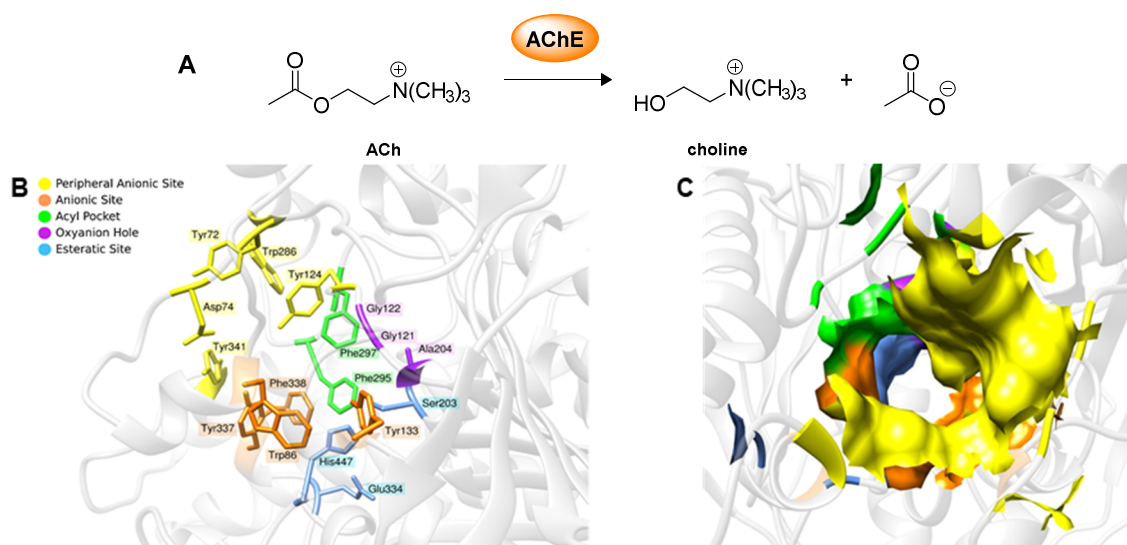


Figure 1. (A) Hydrolysis of acetylcholine (ACh) to choline and acetate catalyzed by acetylcholinesterase (AChE). (B) View of the *h*AChE (PDB:4EY4) active site with key amino acid residues color coded by region (reprinted from [3], with permission from Elsevier). (C) Surface representation of the *h*AChE (PDB:4EY4) active site looking down the gorge with regions color coded as in (B) (reprinted from [3], with permission from Elsevier).

AChE has received considerable attention as a target of chemical intervention, particularly for therapeutic treatment of Alzheimer’s disease (AD). In the United States, AD is the sixth leading cause of death and affects nearly 6 million people, and that number is estimated to grow to nearly 14 million in the next few decades. The disease is characterized by progressive neurodegeneration and diverse symptoms, the most noticeable being cognitive failure (memory loss, language difficulties, inability to plan or problem solve) [10]. The connection between AChE and AD dates back approximately 40 years and is based on the role of ACh in learning and memory and the observation of reduced cholinergic function in the brains of AD patients [11–16]. The logical progression has been to develop an AChE inhibitor(s) (AChEi) to slow the breakdown of ACh and boost its levels (cholinergic hypothesis). Indeed, over the last several decades, four AChEi (tacrine, donepezil, rivastigmine, and galantamine) have all been used to treat AD (Figure 2). A fifth drug used to treat AD, memantine, functions as an *N*-methyl-D-aspartate receptor (NMDAR) antagonist, and it is often used in combination with donepezil. While these drugs have had moderate success in alleviating cognitive symptoms, they are incapable of halting progression or curing AD [17]. This is thought to be, in large part, due to the complex nature and etiology of AD, and it is largely accepted that new and improved AD drugs should target additional factors beyond ACh.

As mentioned above, various other factors are thought to play a role in the AD onset and progression, and there is a significant amount of interplay among these factors and with AChE. The amyloid hypothesis focuses on extracellular aggregates of the amyloid- β ($A\beta$) peptide in the form of oligomers and plaques, which disrupt synaptic transmission and cause neuronal death. The $A\beta$ peptide itself is generated by β -secretase (BACE1) and γ -secretase cleavage of the amyloid precursor protein (APP) [18–22]. $A\beta$ aggregation is promoted through an interaction with the PAS of AChE [23–25] and with metal ions (Cu^{2+} and Zn^{2+}) [26–28]. These metal ions may also, alone or in combination with $A\beta$ oligomers, lead to the production of reactive oxygen species (ROS) and inflammation, which have been implicated in neuronal death and AD progression [29–31]. Dyshomeostasis of other intracellular metal ions, such as Ca^{2+} , may also contribute to neurodegeneration [32,33]. Additionally, metabolic

enzymes such as 15-lipoxygenase (15-LOX), which catalyzes the oxidation of polyunsaturated fatty acids to hydroperoxy acids, and cyclooxygenase-2 (COX-2), which is involved in the conversion of arachidonic acid to prostaglandins, contribute to ROS, oxidative stress, and inflammation [34–37]. Monoamine oxidase (MAO) is also of interest as the increase of monoaminergic neurotransmission through inhibition may alleviate AD symptoms, and ROS-byproducts of the MAO reaction exacerbate oxidative stress [38,39]. Carbonic anhydrase (CA) has even been implicated in AD, and modulation may be beneficial for AD [40,41]. Furthermore, the tau hypothesis focuses on abnormal phosphorylation of the tau protein. This protein is associated with microtubules and interacts with the neuronal cytoskeleton to facilitate intracellular signaling. When hyperphosphorylated, tau can aggregate to form intracellular neurofibrillary tangles (NFTs). This leads to compromised axonal transport and diminished synaptic function, and there is evidence that tau may act synergistically with A β [18,42]. Finally, the mitochondrial cascade hypothesis of AD suggests that the individual genetic makeup determines a baseline mitochondrial function, and the genetics plus environment determines how the mitochondrial function declines with age. The declining mitochondrial function can then initiate other pathologies associated with AD, such as A β aggregation and tau phosphorylation [43,44].

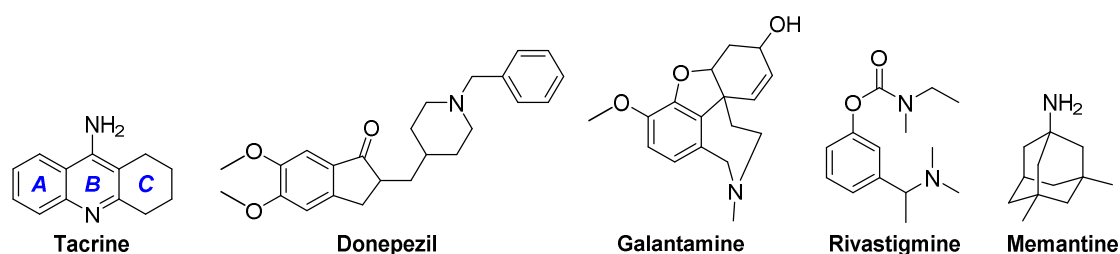


Figure 2. Structures of clinically used Alzheimer’s disease (AD) drugs. Tacrine (discontinued), donepezil, galantamine, and rivastigmine are all AChEi. Memantine is an *N*-methyl-D-aspartate receptor (NMDAR) antagonist. The tricyclic rings of tacrine are labeled A–C for discussion purposes.

Tacrine was the first AChEi approved by the United States Food and Drug Administration for the treatment of AD in 1993. However, it is no longer used clinically due to poor pharmacokinetics requiring four times per day dosing and side effects, the most notorious being hepatotoxicity. Structurally, it is a tricyclic molecule (see Figure 2) consisting of an aromatic *A*-ring, heteroaromatic *B*-ring containing an amino substituent at position 9, and a saturated *C*-ring. Hepatotoxicity has been linked to *A*-ring hydroxylation during metabolism, which is followed by subsequent conversion to a reactive quinone-like metabolite [45–48]. Tacrine has, however, remained an important molecule for research into new AD drugs. This is largely due to its strong inhibition of AChE (low nanomolar IC₅₀), ligand efficiency, synthetic accessibility, tolerance of structural modification, and suitability as a starting point for the multitarget-directed ligand (MTDL) strategy. As mentioned above, AD is multifactorial in nature and new and improved AD drugs should target additional factors beyond the cholinergic system. The MTDL strategy for AD, which aims to combine two or more pharmacophores into a single chemical entity capable of acting on multiple aspects of AD at once, has been implemented using tacrine with varying degrees of success for nearly three decades [49–54]. It should be noted that the MTDL strategy is not unique to AD. For example, it has been applied to the treatment of cancer, malaria, and diabetes [55,56].

Morphy and Rankovic [57] classified MTDLs based on the degree of overlap of the pharmacophores (Figure 3). “Linked” MTDLs contain well separated pharmacophores joined by a distinct linker region that is not present in either parent compound. “Merged” MTDLs represent the opposite end of a continuum where there is a high degree of overlap between the pharmacophores based on structural similarities in the parent compounds. The merged approach often results in smaller and simpler molecules, whereas the linked approach leads to larger, higher molecular weight molecules. The tacrine-based MTDLs reported in the literature are numerous, and our initial survey led us to

divide tacrine-based MTDLs into two groups: Linked and merged. To keep the scope of this manuscript manageable, we report herein only on the merged MTDLs. Furthermore, to focus on current advances, this review details only compounds that were newly reported in the last five years (2015–present). While we recognize the significance of linked tacrine-based MTDLs to this field, we feel that a detailed discussion warrants a separate report, which will be composed in due course.

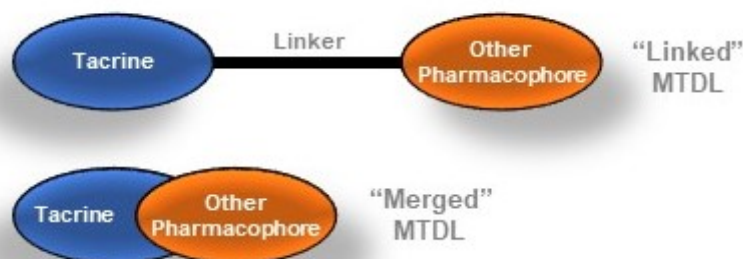


Figure 3. Tacrine-based multitarget-directed ligand (MTDLs) can be classified as “linked” or “merged” based on the degree of overlap of the pharmacophores (adapted with permission from [57], copyright (2005) American Chemical Society).

The merged tacrine-based MTDLs discussed have been grouped based on structural similarities. Special emphasis is placed on the synthesis of the compounds and comparison of *in vitro* AChE inhibition to tacrine, 6-chlorotacrine, or 7-methoxytacrine as appropriate. The 6-chloro substituent on the tacrine scaffold is known to improve the inhibition of AChE while increasing toxicity, and the 7-methoxy substituent, conversely, is known to weaken inhibition while reducing toxicity [58,59]. Unless otherwise stated, inhibition is evaluated using the classic Ellman method [60] with AChE from either *Electrophorus electricus* (*EeAChE*) or human (*hAChE*). These two enzymes have a 56.6% sequence identity, but *EeAChE* is generally the less expensive choice for preliminary testing [61]. We highlight key structure-activity relationship (SAR) trends and *in silico* molecular modeling interactions where appropriate, while also describing relevant secondary *in vitro* and *in vivo* biological activity. Molecular modeling uses either *hAChE* or *Torpedo californica* AChE (*TcAChE*), which have a 51.9% sequence identity [61]. Together, the *in vitro*, *in silico*, and *in vivo* data represent an “in combo” approach to AD drug discovery [56,62].

2. Pyranopyrazole Tacrines

One of the most studied modifications to the tacrine core over the last five years has been the replacement of the aromatic *A*-ring with a fused pyranopyrazole moiety. The resulting 76 different analogs of this tetracyclic scaffold can be divided among two series: **1a–z**, varying in the 4-aryl substituent on the pyran ring, and **2a–ax**, varying at four positions around the scaffold (Scheme 1A) [63–67]. Synthetically, pyranopyrazole tacrines are accessed via closely related two-step sequences (Scheme 1B,C). The pyrano[2,3-*c*]pyrazole core can be constructed using a one-pot four-component reaction between β -ketoesters, hydrazine hydrate or hydrazine derivatives, malononitrile, and aryl or alkyl aldehydes under ultrasonic irradiation in the presence of (*S*)-Pro to give **3a–n** or **4a–o**, **t–aa**, **ae**, **af** [63,64,66]. Alternatively, the pyrano[2,3-*c*]pyrazole core **3o–z** or **4ag–ax** can be constructed from the reaction of 3-methyl-1*H*-pyrazol-5(4*H*)-one or 3-methyl-1-phenyl-1*H*-pyrazol-5(4*H*)-one with aryl aldehydes and malononitrile [65,67]. A subsequent Friedländer reaction with the appropriate cyclohexanone, cycloheptanone, or tetrahydro-4*H*-thiopyran-4-one and AlCl_3 gave the target compounds **1a–z** and **2a–ax** as racemic mixtures.

In addition to acting as AChEi, pyranopyrazole tacrines have shown activity against ROS and $\text{A}\beta$. Among compounds reported by Khoobi et al., the most active inhibitor **1h** (*EeAChE* IC_{50} = 190 nM) showed a slight improvement over tacrine (*EeAChE* IC_{50} = 280 nM) (Table 1). SAR showed that a

methoxy substituent at the 4-position of the phenyl ring showed better inhibition than methyl or fluoro substituents, and a second methoxy group at the 3-position, as seen in **1h**, further improved potency. The Lineweaver-Burk plot showed varying x - and y -intercepts indicating a mixed-type inhibition for this compound (i.e., binding to both the substrate active site (CAS) and a second distinct site (PAS)). Molecular modeling predicted the *R*-enantiomer of **1h** to interact with *TcAChE* near the CAS. The methoxyphenyl group showed a key hydrogen bonding interaction with His440 of the catalytic triad. However, the *S*-enantiomer was predicted to interact with the top of the gorge near the PAS. At 10 μ M, **1h** showed similar neuroprotection to quercetin in response to H_2O_2 -induced damage in PC12 cells [63]. Chioua et al. identified two promising *EeAChEi* in the 4-nitrophenyl analog **1r** (IC_{50} = 170 nM), which was comparable to tacrine (IC_{50} = 190 nM), and the 2-methoxyphenyl analog **1f** (IC_{50} = 1.52 μ M), which was 8-fold less potent than tacrine (Table 1). Interestingly, the Lineweaver-Burk plot indicated that **1f** was a noncompetitive inhibitor, while molecular modeling of (*R*)- and (*S*)-**1r** with *EeAChE* showed similar interactions confined to the PAS, namely π - π stacking interactions between the pyranopyrazole moiety and Trp286 and the pyridine moiety and Tyr341. Furthermore, both **1f** and **1r** showed complete inhibition of $A\beta_{1-40}$ *EeAChE*-induced aggregation at 25 μ M, and they showed comparable neuroprotection against oligomycin A/rotenone-induced oxidative stress in cortical neurons. However, only **1f** was nontoxic to HepG2 cells at 300 μ M and showed favorable in silico CNS permeability [64]. Compounds **1s**, with a para-thioanisole substituent, and **1x**, with a biphenyl substituent, were also highly potent *EeAChEi* being 4.5- to 6-fold more potent than tacrine and having IC_{50} = 58 and 44 nM, respectively (Table 1). Molecular modeling indicated that both enantiomers of **1x** interacted with *TcAChE* at the gorge entrance with the biphenyl substituent positioned towards the CAS [65].

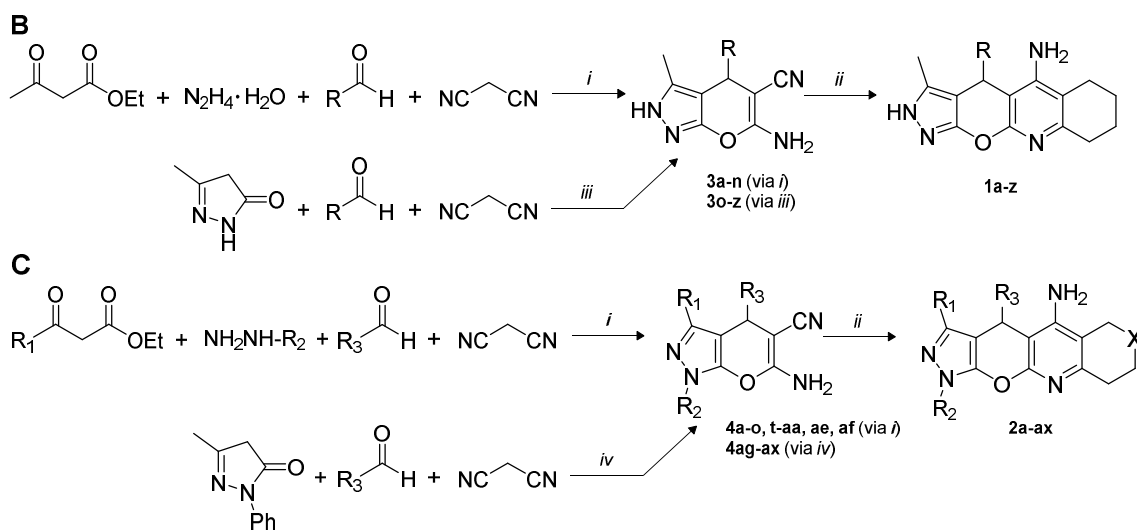
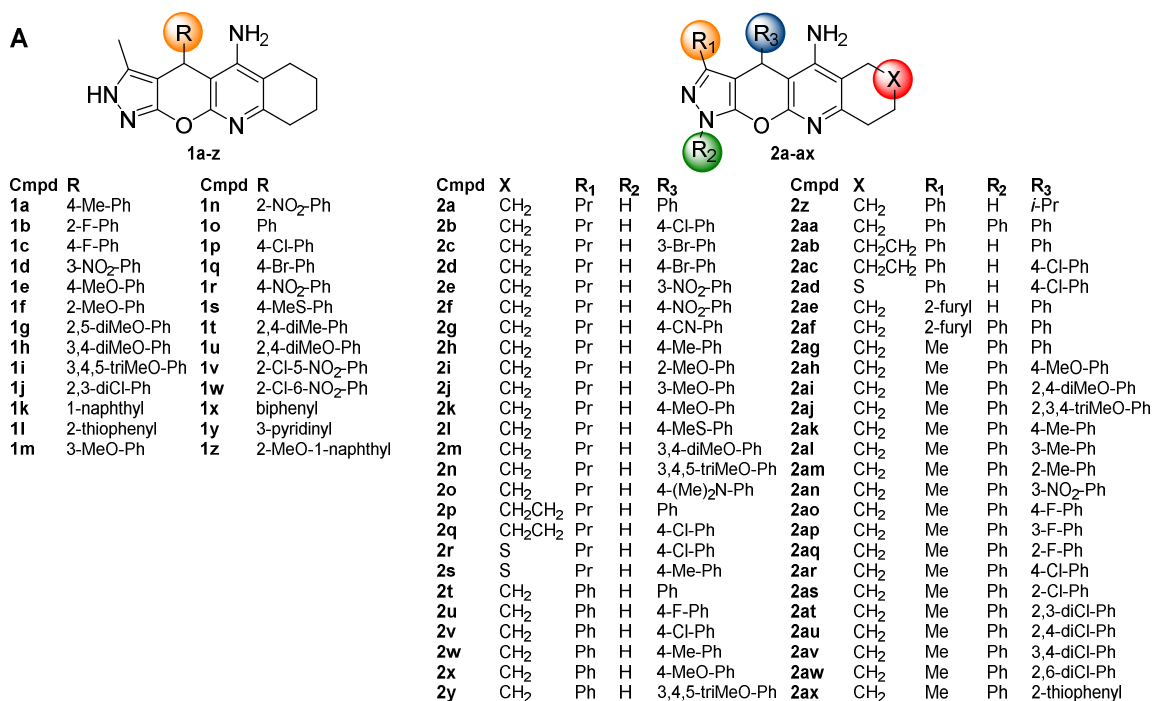
Table 1. Inhibition of *Electrophorus electricus* (*EeAChE*) by pyranopyrazole tacrines **1a–z** (data from [63–65]).

Cmpd	IC_{50} (nM)	Potency Index ¹	Cmpd	IC_{50} (nM)	Potency Index ¹
1a	750 \pm 40	0.37	1n	5040 \pm 1640	0.04
1b	590 \pm 40	0.47	1o	1230 \pm 180	0.21
1c	810 \pm 50	0.35	1p	1660 \pm 270	0.16
1d	3270 \pm 190	0.09	1q	1800 \pm 270	0.14
1e	310 \pm 20	0.90	1r	170 \pm 40	1.12
1f	1520 \pm 490	0.13	1s	58 \pm 5	4.48
1g	500 \pm 30	0.56	1t	290 \pm 30	0.90
1h	190 \pm 10	1.47	1u	260 \pm 50	1.00
1i	2180 \pm 130	0.13	1v	1040 \pm 480	0.25
1j	870 \pm 60	0.32	1w	1770 \pm 190	0.15
1k	320 \pm 20	0.88	1x	44 \pm 2	5.90
1l	720 \pm 40	0.39	1y	330 \pm 30	0.79
1m	5910 \pm 1340	0.03	1z	130 \pm 50	2.00

¹ Compared to tacrine. Potency index = IC_{50} (nM) tacrine/ IC_{50} (nM) cmpd. The red places emphasis on compounds highlighted in the text.

Additional studies have focused on varying ring size on the tacrine core and side chains off of the pyrano[2,3-*c*]pyrazole moiety [66,67]. Compounds **2a–af**, with one exception, all showed IC_{50} < 2 μ M (*EeAChE*). SAR results showed that a propyl or phenyl substituent at R_1 and a 4-methoxyphenyl or 4-fluorophenyl substituent at R_3 gave the best inhibition. Expansion of the tacrine cyclohexane to a cycloheptane gave mixed inhibition results, and bioisosteric replacement of a cyclic methylene with S had little effect. Of note, compared to tacrine (IC_{50} = 221 nM), **2u** (IC_{50} = 34 nM) and **2x** (IC_{50} = 81 nM) were 6- and 3-fold more potent, respectively. Molecular modeling of **2u** with *TcAChE* (Figure 4) showed the pyrazole ring forming key H-bonds with Glu199 and Tyr130 and π - π stacking with Trp84 in the CAS. Additionally, the 4-fluorophenyl moiety was positioned towards the oxyanion hole forming an amide- π stacking interaction with Gly119. The Lineweaver-Burk plot showed a mixed-type inhibition for **2u**. Moreover, **2x** was a moderate inhibitor of 15-LOX (IC_{50} = 31 μ M, compared to quercetin

IC₅₀ = 18 μM), while **2u** showed no inhibition of this enzyme, and both **2u** and **2x** were less hepatotoxic than tacrine, showing no appreciable change in the HepG2 cell viability up to 50 μM [66]. Compounds **2ag–ax** were overall less potent inhibitors of AChE. Of this series, **2ag** and **2ah** with a phenyl and 4-methoxyphenyl substituent off the pyran, respectively, showed the best inhibition of *Ee*AChE with IC₅₀ ~ 2.8 μM [67].



Scheme 1. (A) Structure of pyranopyrazole tacrines **1a–z** and **2a–ax** [63–67]. (B) Synthesis of pyranopyrazole tacrines **1a–z**. (C) Synthesis of pyranopyrazole tacrines **2a–ax**. Reagents and conditions: (i) Ultrasonic irradiation, (S)-Pro, H₂O/EtOH, rt, 10–35 min, 77–95%; (ii) cyclohexanone or cycloheptanone or tetrahydro-4H-thiopyran-4-one, AlCl₃, DCE or DCM, Δ (12–24 h, 65–95%) or MWI (53–90%); (iii) DCE, Δ, 3–4 h, quant.; (iv) DABCO, EtOH, rt, 12 h, quant.

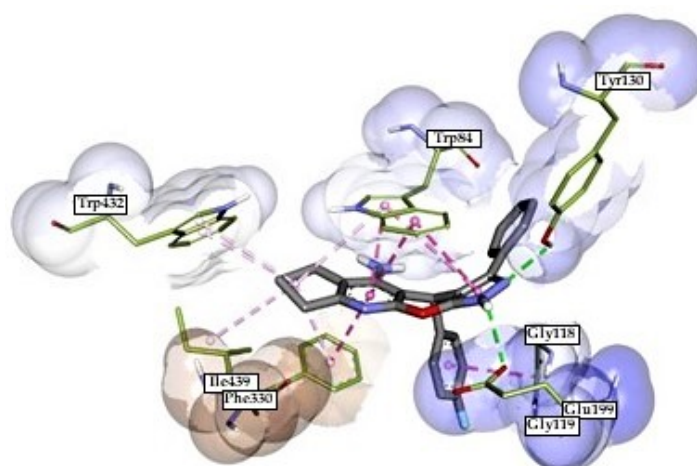
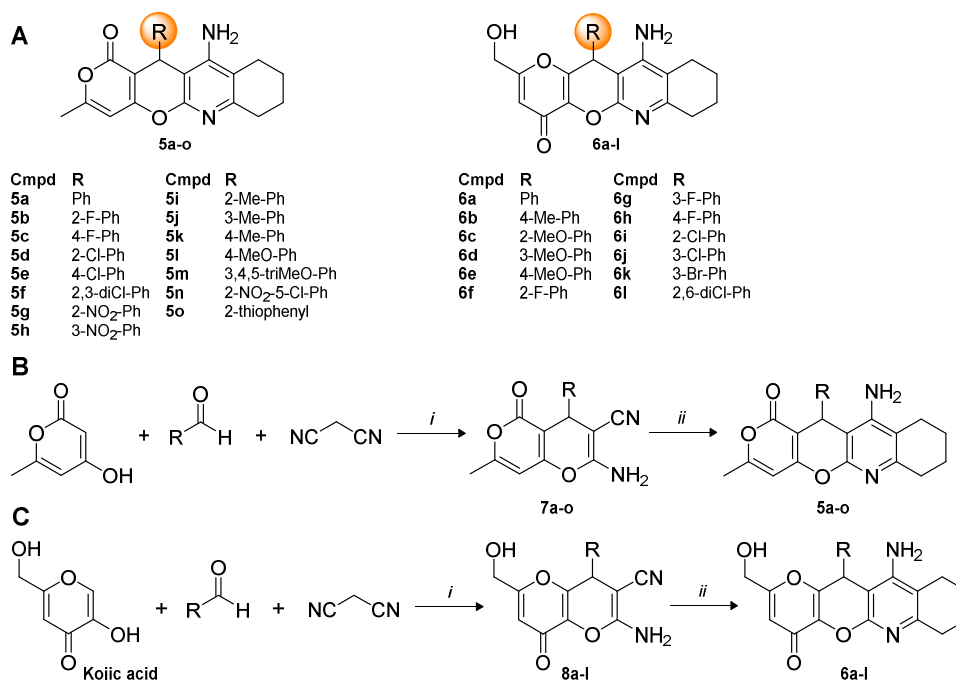


Figure 4. Molecular modeling of **2u** in the substrate active site (CAS) of *TcAChE* (adapted from [66], with permission from Elsevier). The pyrazole ring forms key H-bonds with Glu199 and Tyr130 and π - π stacking with Trp84. The 4-fluorophenyl moiety forms an amide- π stacking interaction with Gly119.

3. Pyranopyranone Tacrines

There have also been recent reports of pyranopyranone tacrines **5a–o** and **6a–l** (Scheme 2A) [68,69]. These compounds contain hydroxypyranone moieties that offer activity against ROS, while maintaining a potent inhibition of AChE. The target compounds were prepared in two steps from a starting hydroxypyranone (Scheme 2B,C). 4-Hydroxy-6-methyl-2*H*-pyran-2-one or kojic acid (KA), a natural fungal metabolite with ROS scavenging ability [70], were reacted with aryl aldehydes and malononitrile in the presence of DABCO or Et₃N to afford intermediate aminocarbonitriles **7a–o** and **8a–l**. Then, the Friedländer reaction with cyclohexanone in the presence of AlCl₃ gave the target compounds **5a–o** and **6a–l** as racemic mixtures [68,69].



Scheme 2. (A) Structure of pyranopyranone tacrines **5a–o** and **6a–l** [68,69]. (B) Synthesis of pyranopyranone tacrines **5a–o**. (C) Synthesis of pyranopyranone tacrines **6a–l**. Reagents and conditions: (i) DABCO (rt, 12 h, quant.) or Et₃N (Δ , 5 min, 63–77%), EtOH, rt; (ii) cyclohexanone, AlCl₃, DCE or 1,4-dioxane, Δ , 2–18 h, 50–87%.

Compared to tacrine (*EeAChE* IC₅₀ = 48 nM), **5a–o** showed a weaker inhibition. The most potent compound **5f** with a 2,3-dichlorophenyl group was 8-fold weaker (*EeAChE* IC₅₀ = 370 nM). **5f** also showed moderate neuroprotection in PC12 cells against H₂O₂-induced damage, but it did not perform as well as quercetin in the same assay. The Lineweaver-Burk plot of **5f** showed a mixed inhibition, suggesting an interaction with both the CAS and PAS. Interestingly, molecular modeling showed that the *R*-enantiomer of **5f** was predicted to interact with the PAS, while the *S*-enantiomer was predicted to interact with the mid-gorge region and span the PAS-CAS distance [68]. Similarly, **6a–l** also showed a comparatively weaker inhibition. Of this series, the most potent inhibitor of *EeAChE* was the 3-methoxyphenyl substituted **6d** (IC₅₀ = 640 nM), which was 20-fold less potent than tacrine (IC₅₀ = 31 nM). Promisingly though, most of these compounds were significantly less toxic than tacrine. In addition, **6d** maintained a 65.5% viability in HepG2 cells at 1 mM, 6-fold less toxic than tacrine (10.9% viability at 1 mM). Moreover, **6d** improved upon the known antioxidant capacity of KA (ORAC assay; 4.79 and 2.51 Trolox equivalents for **6d** and KA, respectively), and it showed a capable neuroprotection against oligomycin/rotenone and Aβ₁₋₄₀ in SH-SY5Y cells at 3 μM. Molecular modeling of *hAChE* with **6d** *R*- and *S*-enantiomers indicated an association of both with the PAS via π-π stacking with Trp286 and Tyr341, acting as a barrier to the active site of the enzyme (Figure 5). Additional key H-bonds were noted, including the primary hydroxyl group for both enantiomers with Tyr72 and the tacrine-like amino group with Tyr124 (*R*-enantiomer) or Asp74 (*S*-enantiomer) [69].

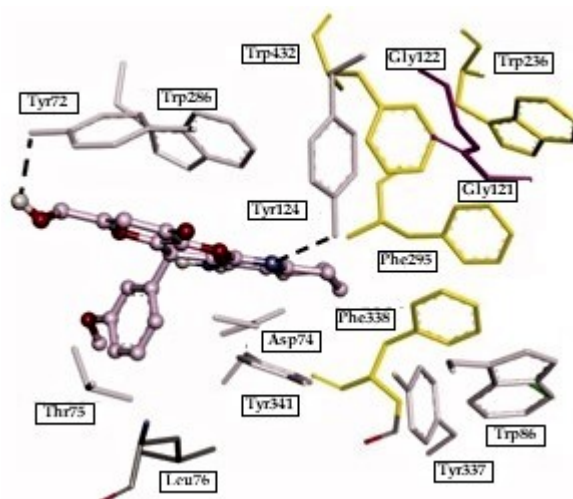
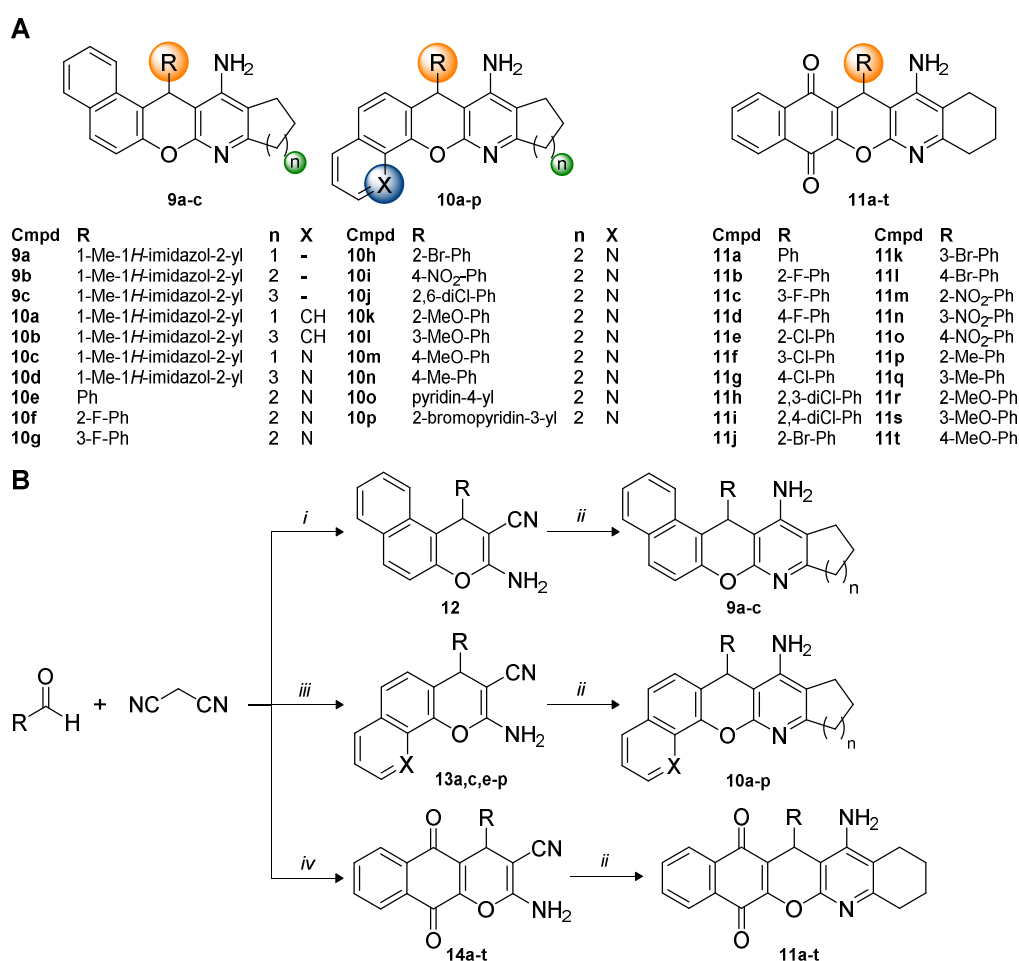


Figure 5. Molecular modeling of (*R*)-**6d** in the second distinct site (PAS) of *hAChE* (adapted from [69]). Important interactions include π-π stacking with Trp286 and Tyr341 and H-bonds of the primary hydroxyl group with Tyr72 and the tacrine-like amino group with Tyr124.

4. Pyranonaphthalene, Pyranoquinoline, and Pyranonaphthoquinone Tacrines

Pentacyclic pyranotacrines bearing a fused naphthalene, quinoline, or naphthoquinone moiety (Scheme 3A) have shown diverse anti-AD activity, including AChE inhibition, BACE1 inhibition, ROS scavenging, and metal chelation [71–74]. The pyranoquinoline tacrines were designed to incorporate the hydroxyquinoline moiety of cliquinol, a known antioxidant and Cu-chelator [72,75], while the pyranonaphthoquinone tacrines were designed to incorporate the known 1,4-naphthoquinone BACE1i scaffold [73,76]. The compounds were prepared through closely related two-step sequences relying on 4*H*-pyran construction from malononitrile, aryl aldehydes, and either 2-naphthol, 1-naphthol, 8-hydroxyquinoline, or 2-hydroxy-1,4-naphthoquinone to give intermediates **12** [71], **13a,c,e–p** [71,72], and **14a–t** [73,74] (Scheme 3B). In all cases, a subsequent Friedländer reaction with the appropriate cycloalkanone and AlCl₃ gave the target compounds **9a–c**, **10a–p**, and **11a–t** as racemic mixtures.



Scheme 3. (A) Structure of pyranonaphthalene (**9a–c**, **10a,b**), pyranoquinoline (**10c–p**), and pyranonaphthoquinone tacrines **11a–t** [71–74]. (B) Synthesis of pyranonaphthalene (**9a–c**, **10a,b**), pyranoquinoline (**10c–p**), and pyranonaphthoquinone tacrines **11a–t**. Reagents and conditions: (i) 2-Naphthol, piperidine, EtOH, Δ , 12 h, 72%; (ii) cyclopentanone or cyclohexanone or cycloheptanone, AlCl₃, DCE or 1,4-dioxane, Δ (2–24 h, 40–95%) or MWI (3 h, 9–70%); (iii) 1-naphthol or 8-hydroxyquinoline, piperidine, EtOH, Δ , 15 min–12 h, 47–93%; (iv) 2-hydroxy-1,4-naphthoquinone, piperidine, EtOH, Δ , 2–6 h, quant.

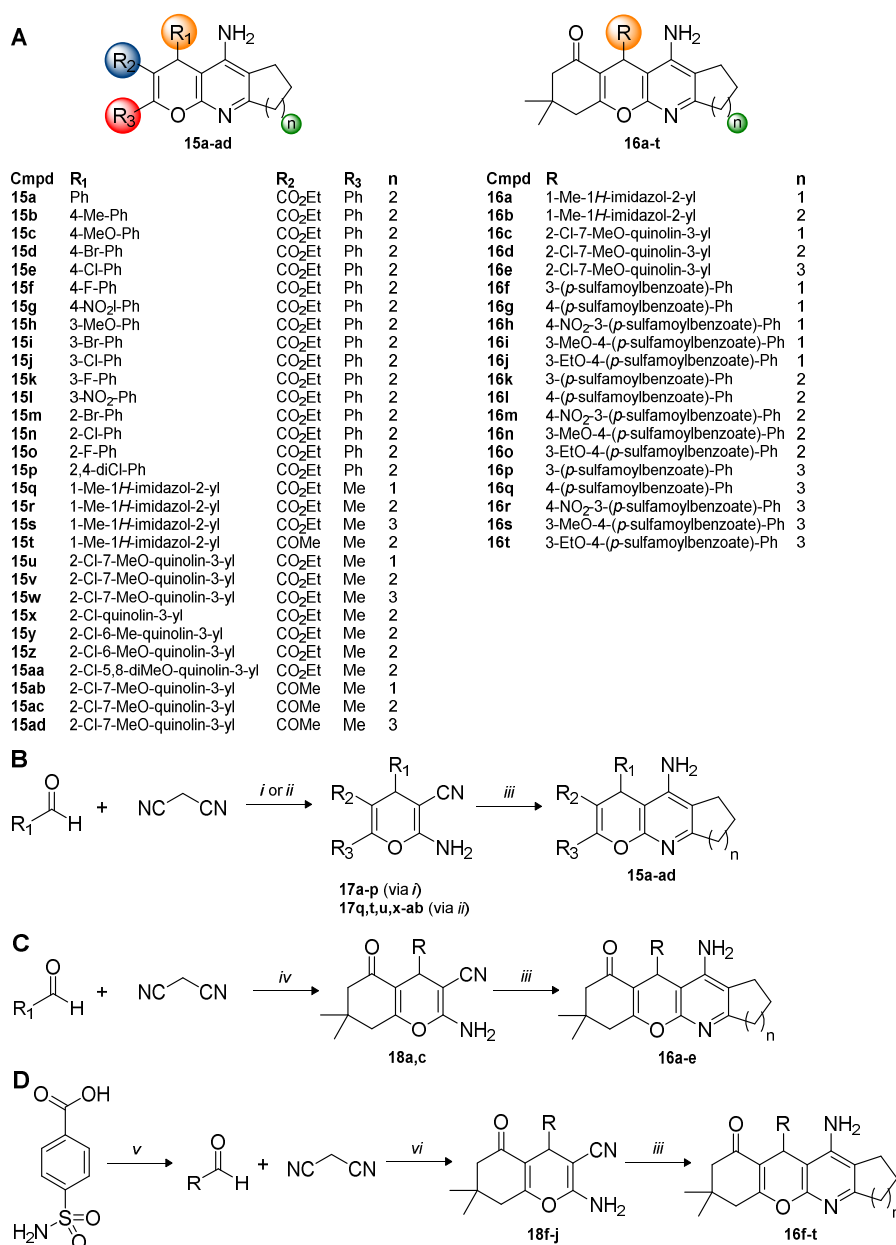
In terms of biological activity, these compounds showed a weak inhibition of AChE with varying secondary activity. Among pyranonaphthalene and pyranoquinoline tacrines bearing a 1-methyl-1*H*-imidazol-2-yl substituent **9a–c** and **10a–d**, compared to tacrine (*Ee*AChE IC₅₀ = 89.8 nM), all were weaker inhibitors of AChE. Even the most potent inhibitor **9b** (*Ee*AChE IC₅₀ = 6.73 μ M) was 75-fold less potent than tacrine. Non-competitive inhibition was indicated by the Lineweaver-Burk plot and confirmed by molecular modeling, which showed both enantiomers of **9b** favoring an interaction with the PAS. The antioxidant capacity was promising, however, with compounds exhibiting between 1.47–2.75 Trolox equivalents by the ORAC assay, but **9b** did show increased hepatotoxicity compared to tacrine in HepG2 cells [71]. Among **10e–p**, **10l** bearing a 3-methoxyphenyl substituent was the most potent against *Ee*AChE (IC₅₀ = 40 nM, compared to tacrine IC₅₀ = 30 nM). SAR indicated the phenyl substituted inhibitors to be more potent than the pyridinyl substituted ones. The Lineweaver-Burk plot showed that **10l** acted as a noncompetitive inhibitor of *h*AChE. Molecular modeling predicted that the *R*-enantiomer bound to *h*AChE at the PAS primarily through π - π stacking interactions. Moreover, noted were two H-bonds between the 8-amino group and Asp74 and Leu76. The *S*-enantiomer was predicted to bind in a similar fashion. These compounds showed a moderate antioxidant ability, and **10l**, although not the best antioxidant tested, gave an ORAC assay result of 1.83 Trolox equivalents.

In addition, **10l** was non-toxic in HepG2 cells at concentrations up to 1 mM and was predicted to cross the blood-brain barrier (BBB) by the parallel artificial membrane permeability assay (PAMPA) (effective permeability (P_e) = 5.41×10^{-6} cm/s where a high BBB permeation predicted with P_e (10^{-6} cm/s) > 4.0, a low BBB permeation predicted with P_e (10^{-6} cm/s) < 2.0, and BBB permeation uncertain with P_e (10^{-6} cm/s) from 2.0 to 4.0). Disappointingly, **10l** showed not ability to chelate Cu^{2+} or Fe^{2+} [72]. The pyranonaphthoquinone tacrines **11a–t** showed significantly less inhibition of AChE than tacrine. The 3-nitrophenyl substituted **11n** ($EeAChE$ IC_{50} = 860 nM) was 17-fold less potent than tacrine ($EeAChE$ IC_{50} = 50 nM) [73], and the 4-methoxyphenyl substituted **11t** ($hAChE$ IC_{50} = 1.10 μM) was 8.5-fold less potent than tacrine ($hAChE$ IC_{50} = 130 nM) [74]. **11n** and **11t** showed a mixed-type inhibition by the Lineweaver-Burk plot analysis, while molecular modeling with $TcAChE$ showed a similar interaction for both compounds with CAS and PAS residues. Key interactions included π - π interactions with the aromatic rings and Phe330 and Trp84 in the CAS, as well as an H-bond between the nitro substituent (for **11n**) and Tyr334 in the PAS [73,74]. Additionally, **11n** showed a promising ability to chelate Cu^{2+} , Zn^{2+} , and Fe^{2+} . Unfortunately though, **11n** showed only a weak BACE1 inhibition compared to the known peptidomimetic BACE1 inhibitor OM99-2 (IC_{50} = 19.60 μM and 14 nM, respectively), and it showed no antioxidant activity or neuroprotective ability against $A\beta_{25-35}$ [73]. Importantly, **11t** showed 3.5-fold less hepatotoxicity than tacrine at 1 mM in HepG2 cells and was predicted to be CNS active (PAMPA-BBB, P_e = 4.4×10^{-6} cm/s) [74].

5. Other Pyranotacrines

Other tri- and tetracyclic pyranotacrines with a diverse anti-AD activity have been studied (Scheme 4A) [71,77–79]. The 4*H*-pyran core was formed by either a one-step reaction of ethyl benzoylacetate with benzaldehyde derivative and malononitrile in the presence of piperidine (in the case of **17a–p** [77]) or a two-step sequence in which the appropriate imidazole- or quinolinecarboxaldehyde was first condensed with malononitrile and then treated with a 1,3-dicarbonyl (in the case of **17q,t,u,x–ab**, and **18a,c**) in the presence of piperidine (Scheme 4B,C) [71,78]. Alternatively, for the sulfamoyl-containing pyranotacrines **16f–t**, SOCl_2 and microwave irradiation was first used to make *p*-sulfamoylbenzoyl chloride from the corresponding acid. Esterification with hydroxybenzaldehydes then gave sulfamoylbenzoate benzaldehydes, which were subjected to a three-component Aldol-Michael-cyclization sequence with malononitrile and dimedone under microwave irradiation to give intermediates **18f–j** (Scheme 4D) [79]. In all cases, a final Friedländer reaction with the appropriate cycloalkanone in the presence of AlCl_3 gave the target compounds **15a–ad** and **16a–t** as racemic mixtures (Scheme 4B–D).

Eghtedari et al. found that all compounds **15a–p** showed IC_{50} values ($EeAChE$) < 6 μM . The best inhibitor **15i**, bearing a R_1 3-bromophenyl substituent was 5-fold more potent than tacrine with an IC_{50} = 69 nM and showed a mixed-type inhibition based on the Lineweaver-Burk plot. SAR suggested that the best inhibition was achieved with a R_1 2- or 3-bromo/chlorophenyl substituent. Molecular modeling predicted **15i** to bind to the CAS of AChE near the catalytic triad. The predominant binding interaction was predicted to be the hydrophobic/ π - π interactions, but an H-bond between the amino group and His440 was also noted. While **15i** was predicted to cross the BBB (0.80 probability by the online admetSAR server), it was only weakly neuroprotective against H_2O_2 -induced injury in PC12 cells and was moderately toxic to HepG2 cells (but still less toxic than tacrine) [77]. All synthesized sulfamoyl-containing pyranotacrines **16f–t** were potent $EeAChE$ (IC_{50} < 150 nM), but **16l** was the most potent (IC_{50} = 10 nM) and was 5.5-fold more potent than tacrine (IC_{50} = 55 nM) (Table 2). In general, the cyclohexyl moiety was favored over the cyclopentyl and cycloheptyl derivatives, and the *p*-sulfamoylbenzoate moiety was favored at the 4-position among this series. However, no molecular modeling or X-ray crystallography was performed to visualize the interaction of the inhibitors with the enzyme. Of the 15 compounds evaluated, 10 showed some degree of antioxidant activity [79].



Scheme 4. (A) Structure of other pyranotacrines **15a–ad** and **16a–t** [71,77–79]. (B) Synthesis of pyranotacrines **15a–ad**. (C) Synthesis of pyranotacrines **16a–e**. (D) Synthesis of sulfamoyl-containing pyranotacrines **16f–t**. Reagents and conditions: (i) Ethyl benzoylacetate ($R_2 = \text{CO}_2\text{Et}$, $R_3 = \text{Ph}$), piperidine, EtOH, Δ , 3 h, quant.; (ii) ethyl acetoacetate ($R_2 = \text{CO}_2\text{Et}$, $R_3 = \text{Me}$) or acetylacetone ($R_2 = \text{COMe}$, $R_3 = \text{Me}$), piperidine, EtOH, rt, 12 h, 78–93%; (iii) cyclopentanone or cyclohexanone or cycloheptanone, AlCl_3 , DCE or toluene, Δ (3–24 h, 32–87%) or MWI (10 min, 70–83%); (iv) dimedone, piperidine, EtOH, rt, 12 h, 69–76%; (v) (a) SOCl_2 , MWI, 30 min, 88%; (b) hydroxybenzaldehyde derivative, pyridine, DCM, rt, 12 h, 85–93%; (vi) dimedone, K_2CO_3 , EtOH, MWI, 6 min, 85–89%.

However, modification to the imidazo- or quinolinopyranotacrines was found to weaken the inhibition. For example, compared to tacrine ($EeAChE$ $\text{IC}_{50} = 89.8$ nM), all imidazopyranotacrines **15q–t** and **16a,b** (Table 2) were weaker inhibitors of AChE [71]. For the quinolinopyranotacrines, constructed due to the prevalence of the 2-chloroquinolin-3-yl moiety in many pharmacologically active compounds, the most potent AChEi were **15x** and **15ac** ($EeAChE$ $\text{IC}_{50} = 480$ and 470 nM, respectively, compared to tacrine $\text{IC}_{50} = 190$ nM) [78]. While lacking as AChEi, imidazo- and quinolinopyranotacrines have other beneficial properties. All of the imidazopyranotacrines showed

high antioxidant capacity, with all but one compound exhibiting between 1.70–2.34 Trolox equivalents by the ORAC assay. Imidazopyranotacrine **15t**, despite a weak AChE inhibition ($IC_{50} = 38.7 \mu\text{M}$), was particularly promising given its high antioxidant capacity and low hepatotoxicity compared to tacrine in HepG2 cells (non-toxic at 1 mM) [71]. In addition, **15ac** was able to significantly inhibit *Ee*AChE-induced $A\beta_{1-40}$ aggregation, and both **15x** and **15ac** were less hepatotoxic than tacrine in HepG2 cells, with **15x** being 27-fold less toxic. Moreover, **15x** and **15ac** showed promising neuroprotection in SH-SY5Y cells against oxidative stress, $A\beta_{1-40}$ aggregation, and tau-phosphorylation [78].

Table 2. Inhibition of *Ee*AChE by pyranotacrines **16a–t** (data from [71,78,79]).

Cmpd	IC_{50} (nM)	Potency Index ¹	Cmpd	IC_{50} (nM)	Potency Index ¹
16a	>10 μM	-	16k	41 \pm 2	1.34
16b	>10 μM	-	16l	10 \pm 1	5.50
16c	580 \pm 140	0.33	16m	20 \pm 3	2.75
16d	>10 μM	-	16n	90 \pm 7	0.61
16e	2810 \pm 880	0.07	16o	120 \pm 7	0.46
16f	140 \pm 6	0.39	16p	110 \pm 70	0.50
16g	20 \pm 1	2.75	16q	80 \pm 3	0.69
16h	130 \pm 5	0.42	16r	70 \pm 2	0.79
16i	140 \pm 2	0.39	16s	134 \pm 40	0.41
16j	32 \pm 3	1.72	16t	82 \pm 9	0.67

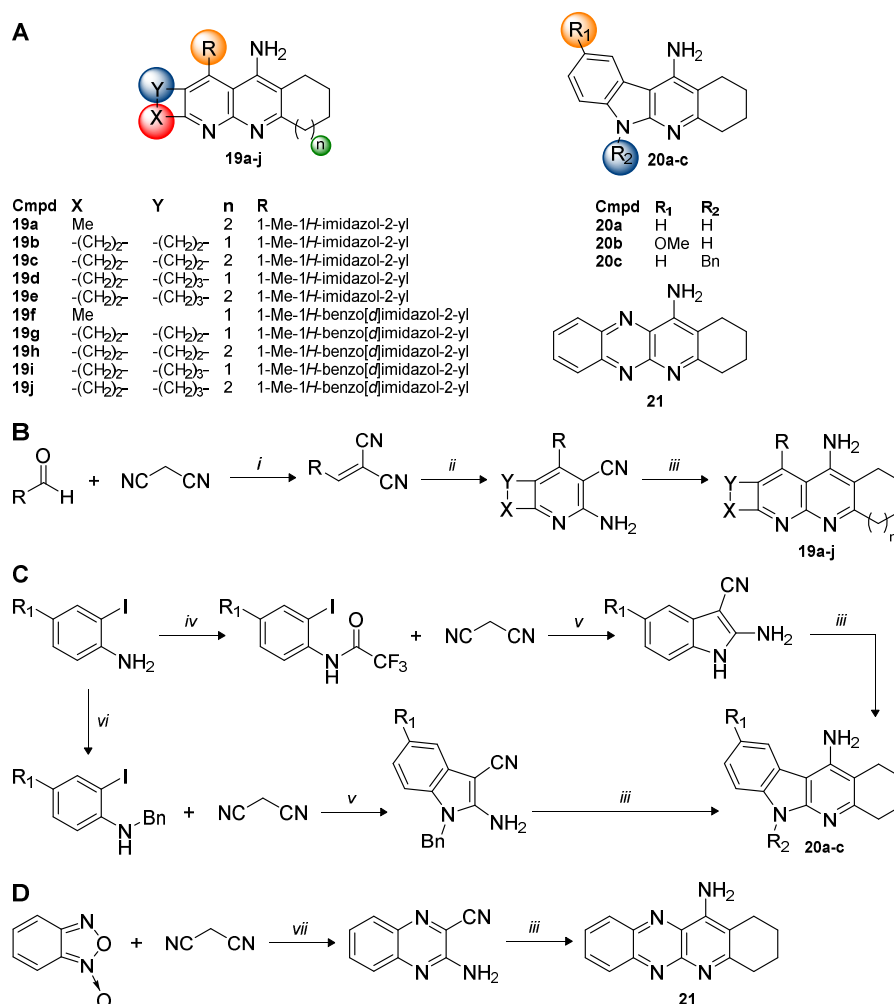
¹ Compared to tacrine. Potency index = IC_{50} (nM) tacrine/ IC_{50} (nM) cmpd. The red places emphasis on compounds highlighted in the text.

6. Pyridino-, Indolo-, and Quinoxalinotacrines

Replacement of the aromatic *A*-ring of tacrine with nitrogen heterocycles has resulted in pyridino-, indolo-, and quinoxalinotacrines (Scheme 5A) [80–82]. Pyridinotacrines **19a–j** were prepared from 1-methyl-1*H*-(benz)imidazol-2-carbaldehyde by condensation with malononitrile followed by a reaction with the appropriate enolizable ketone (acetone, cyclohexanone, or cycloheptanone) and NH_4OAc in AcOH to yield 2-amino-3-cyanopyridine intermediates. The Friedländer reaction with the appropriate cycloalkanone in the presence of AlCl_3 gave the target compounds (Scheme 5B) [80]. Indolotacrines **20a–c** were designed to fuse a 2-aminoindole-3-carbonitrile scaffold, which contains common pharmacophores of MAOi, and tacrine/7-methoxytacrine. The starting commercially available or easily made 2-iodoanilines could either be trifluoroacetylated with TFAA or benzylated with reductive amination using benzaldehyde and NaBH_3CN . In either case, the 2-aminoindole-3-carbonitrile core was formed via Cu-catalyzed cyclization with malononitrile, which, upon the tFriedländer reaction with cyclohexanone and AlCl_3 gave the desired compounds (Scheme 5C) [81]. Quinoxalinotacrine **21** was prepared from the Friedländer reaction between 3-amino-2-quinoxalinecarbonitrile [83] and cyclohexanone in the presence of AlCl_3 [82].

Modification to these *N*-heterocyclic tacrine scaffolds generally comes with a reduction in AChE inhibition and mixed other properties. For example, all pyridinotacrines **19a–j** reported by Boulebd et al. [80] showed a weaker inhibition of *Ee*AChE than tacrine ($IC_{50} = 30 \text{ nM}$), albeit over a fairly narrow range with $IC_{50} = 310–620 \text{ nM}$. While not the most potent AChEi, compound **19d** ($IC_{50} = 500 \text{ nM}$) is noteworthy in that it showed no toxicity to HepG2 cells at concentrations as high as 1 mM. The authors hypothesized that reduced toxicity compared to tacrine was due to the fully substituted pyridine ring (no C-H bonds), which blocked oxidation to the reactive iminoquinone metabolite associated with hepatotoxicity in tacrine. However, none of the synthesized compounds displayed significant antioxidant activity [80]. Indolotacrine **20b** showed that *h*AChE $IC_{50} = 1.5 \mu\text{M}$, making it more potent than 7-methoxytacrine ($IC_{50} = 10 \mu\text{M}$) but less potent than tacrine ($IC_{50} = 320 \text{ nM}$). In addition, **20b** showed a promising inhibition of MAO-A ($IC_{50} = 490 \text{ nM}$) and was predicted to cross the BBB (PAMPA- BBB , $P_e = 6.6 \times 10^{-6} \text{ cm/s}$), but it lacked antioxidant activity and was more cytotoxic to a CHO-K1 cell line and more hepatotoxic to a HepG2 cell line than both tacrine and

7-methoxytacrine [81]. Lastly, compared to tacrine (*hAChE* IC₅₀ = 374 nM), quinoxalinotacrine **21** was a significantly weaker *hAChE* inhibitor (IC₅₀ = 22.0 μM). Molecular modeling predicted **21** interacted with *hAChE* in the mid-gorge region with the cyclohexyl ring oriented toward the CAS forming alkyl- π interactions with Trp86 and the phenyl and pyridinyl rings oriented towards the PAS forming π - π interactions with Tyr341 and Tyr337, respectively. Moreover, noted were key H-bonds between the amino group and pyrazine nitrogen and Tyr124 and Asp74. An initial in silico analysis predicted **21** had favorable ADME properties for CNS action (MW < 450, hydrogen-bond donors < 3, hydrogen-bond acceptors < 7, number of hydrogen bond donor < 5, Van der Waals surface area of polar nitrogen and oxygen atoms < 90, number of rotatable bonds < 8, hydrogen bonds < 8, logBB = -0.332) and that **21** (and 10 possible metabolites) showed no potential hepatotoxicity. Subsequent screening in HepG2 cells showed that **21** first showed a significant reduction in cell viability at 300 μM (for comparison, tacrine showed a significant reduction in cell viability at 30 μM). Additionally, **21** showed neuroprotection in SH-SY5Y cells against ROS (oligomycin A/rotenone-induced) and tau hyperphosphorylation (okadaic acid-induced) at concentrations as low as 0.1 μM, but the effect diminished above 1 μM [82].



Scheme 5. (A) Structure of pyridino- (**19a–j**), indolo- (**20a–c**), and quinoxalinotacrine **21** [80–82]. (B) Synthesis of pyridinotacrine **19a–j**. (C) Synthesis of indolotacrine **20a–c**. (D) Synthesis of quinoxalinotacrine **21**. Reagents and conditions: (i) Piperidine, EtOH, rt; (ii) acetone or cyclohexanone or cycloheptanone, NH₄OAc, AcOH, Δ ; (iii) cyclohexanone or cycloheptanone, AlCl₃, DCE, Δ (18 h, 72–95%) or MWI (2 h, 16–88%); (iv) TFAA, TEA, THF, rt, 12 h, 97–99%; (v) *L*-Pro or picolinic acid, K₂CO₃, CuI, DMSO/H₂O, 60 °C (12 h, 48–90%) or MWI (12 h, 26%); (vi) (a) benzaldehyde, MeOH, rt, 12 h, 97%; (b) NaBH₃CN, AcOH/MeOH, rt, 12 h, 75%; (vii) (a) TEA, DMF, rt, 1.5 h, 75%; (b) Na₂S₂O₄, H₂O/MeOH, 50 °C, 3 h, 87% [83].

7. Pyrrolo-, Pyrazolo-, and Furanotacrines; Pyrazolophthalazine Tacrines

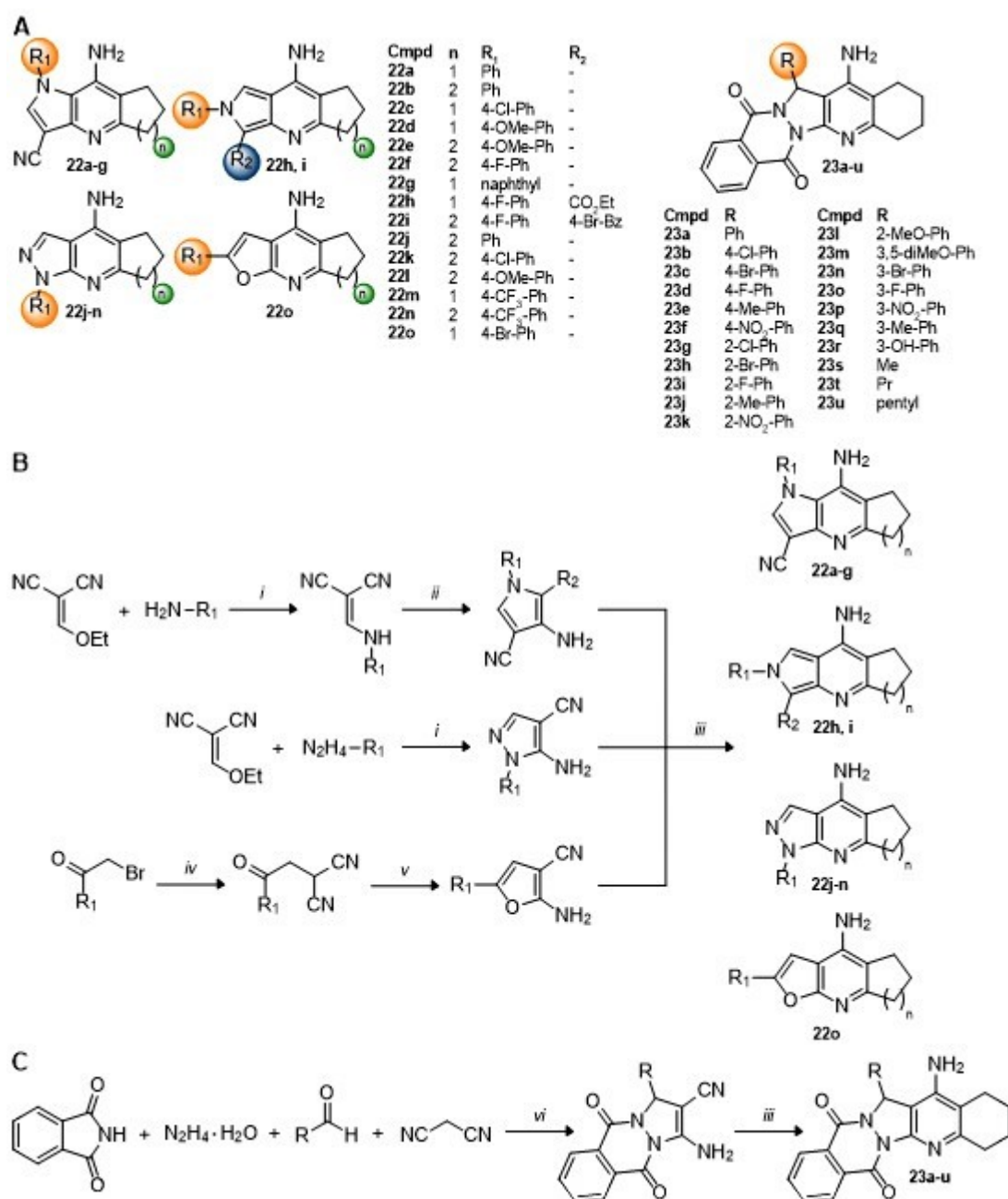
Again, replacement of the aromatic *A*-ring of tacrine with other nitrogen and oxygen heterocycles has resulted in pyrrolo-, pyrazolo-, and furanotacrines, as well as pyrazolophthalazine tacrines (Scheme 6A) [84,85]. The pyrrolotacrine series **22a–i** was constructed starting from ethoxymethylene malononitrile by a reaction with aromatic amines to form arylaminomalonnitriles, which could undergo Thorpe-Ziegler cyclization to the pyrrole upon reaction with chloroacetonitrile, 4-bromophenacylbromide, or ethyl bromoacetate and TEA. A final Friedländer reaction with cycloalkanones and AlCl₃ under microwave irradiation gave the target 2,3-fused pyrrolotacrines **22a–g** or 3,4-fused pyrrolotacrines **22h,i** (Scheme 6B). Likewise, the pyrazolo series was also constructed starting from ethoxymethylene malononitrile by a reaction with aromatic hydrazines to form the 5-amino-4-cyanopyrazoles followed by the Friedländer reaction with cycloalkanones and AlCl₃ under microwave irradiation gave the target 3,4-fused pyrazolotacrines **22j–n** (Scheme 6B). The furanotacrine **22o** was constructed starting from malononitrile by initial alkylation with 4-bromophenacylbromide and then cyclization with TEA to the 2-amino-3-cyanofuran. A final Friedländer reaction with cyclopentanone as before gave the target compound (Scheme 6B) [84]. For **23a–u**, the pyrazolo[1,2-*b*]phthalazine core was constructed using a one-pot, Ni-catalyzed, four-component reaction with phthalimide, hydrazine hydrate, malononitrile, and benzaldehyde derivatives. A subsequent Friedländer reaction with cyclohexanone and AlCl₃ gave the desired products as racemic mixtures (Scheme 6C) [85].

Compounds **22a–o** were shown to be potent AChEi, as all compounds presented IC₅₀ values (enzyme source not specified) between 4.06–6.87 nM that are comparable to donepezil (IC₅₀ = 7.23 nM). There seems to be little difference between the pyrrolo-, pyrazolo-, and furanotacrines in regards to the inhibitory activity, and no additional biological properties were examined [84]. A more in depth analysis was performed on pyrazolophthalazine tacrines **23a–u**. Of the compounds synthesized, five showed very potent inhibition (*Ee*AChE IC₅₀ < 100 nM) with **23o** (IC₅₀ = 23 nM), bearing a *m*-fluorophenyl substituent, and **23i** (IC₅₀ = 49 nM), bearing an *o*-methoxyphenyl substituent, being the most potent and being 16-fold and 7.5-fold more potent than tacrine, respectively (Table 3). SAR showed that the phenyl substituted compounds outperformed the alkyl substituted ones, and *o/m/p*-substituted phenyl substituents outperformed the non-substituted phenyl counterpart. The Lineweaver-Burk plot showed that **23i** as a mixed-type inhibitor, and theoretical calculations predicted it to be CNS active (0.9260 probability by the online admetSAR server). Molecular modeling showed the *R*-enantiomer of **23i** to interact more favorably with *Tc*AChE, specifically at the PAS via the π - π stacking with Tyr120 and Trp278 and H-bonding with Tyr69. Additionally, **23i** showed that the moderate ability to inhibit both self- and AChE-induced A β aggregation, was less toxic than tacrine with HepG2 cell viability remaining high (83%) at 300 μ M, and exhibited a slight antioxidant activity as it protected PC12 cells from H₂O₂-induced death at 100 μ M [85].

Table 3. Inhibition of *Ee*AChE by pyrazolophthalazine tacrines **23a–u** (data from [85]).

Cmpd	IC ₅₀ (nM)	Potency Index ¹	Cmpd	IC ₅₀ (nM)	Potency Index ¹
23a	614	0.59	23l	49	7.45
23b	60	6.08	23m	3370	0.11
23c	80	4.56	23n	271	1.35
23d	69	5.29	23o	23	15.9
23e	100	3.65	23p	140	2.61
23f	310	1.18	23q	467	0.78
23g	592	0.62	23r	160	2.28
23h	599	0.61	23s	2150	0.17
23i	618	0.59	23t	1630	0.22
23j	193	1.89	23u	612	0.60
23k	280	1.30			

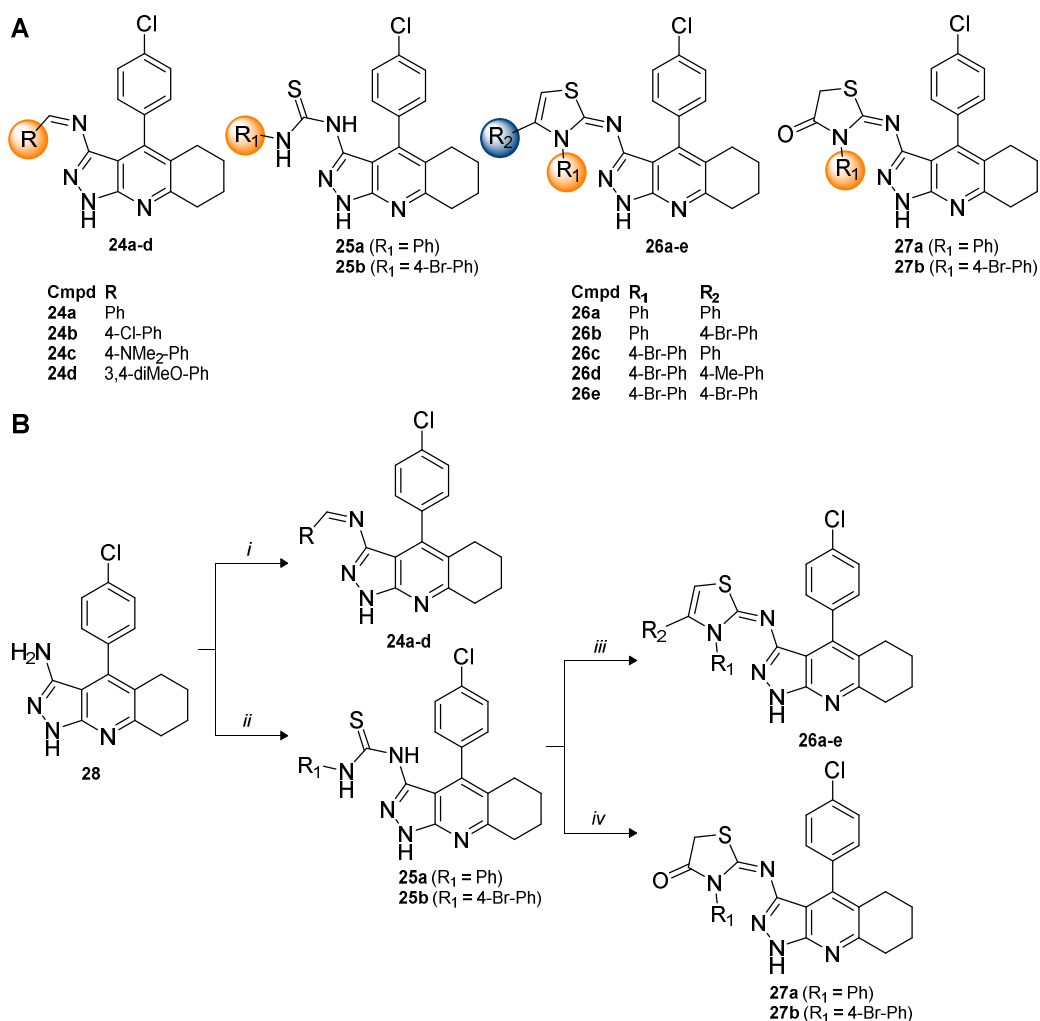
¹ Compared to tacrine. Potency index = IC₅₀ (nM) tacrine/IC₅₀ (nM) cmpd. The red places emphasis on compounds highlighted in the text.



Scheme 6. (A) Structure of pyrrolo- (22a–i), pyrazolo- (22j–n), and furanotacrines 22o, as well as pyrazolophthalazine tacrines 23a–u [84,85]. (B) Synthesis of pyrrolo- (22a–i), pyrazolo- (22j–n), and furanotacrines 22o. (C) Synthesis of pyrazolophthalazine tacrines 23a–u. Reagents and conditions: (i) EtOH, rt, 30 min, >80%; (ii) X-CH₂-R₂ (where X = Cl or Br, Y = CN, CO₂Et, or 4-Br-Bz) TEA, Δ, 15–30 min, 63–91%; (iii) cyclopentanone or cyclohexanone, AlCl₃, DCE or DCM, Δ (8–24 h, 30–95%) or MWI (30–32 min, 45–87%); (iv) malononitrile, 10% KOH, EtOH, rt, 30 min, 80%; (v) TEA, EtOH, Δ, 2 h, 67%; (vi) NiCl₂·6H₂O, EtOH, Δ, 4 h.

An additional series of pyrazolotacrines **24a–d**, **25a,b**, **26a–e**, and **27a,b** have been very recently reported (Scheme 7A) [86]. The design rationale for these compounds was to merge the 4-chlorophenyltetrahydroquinoline moiety for AChE inhibition with the pyrazole and thiourea moieties of known COX-2 inhibitors (e.g., celecoxib) to potentially modulate the ACh and ROS/inflammatory aspects of AD. Starting from previously prepared amino pyrazolotacrines **28** [87], condensation with benzaldehyde derivatives or phenyl isothiocyanates gave the imines **24a–d** and

thioureas **25a,b**. A further reaction of **25a,b** with phenacyl bromides or ethyl bromoacetate afforded the thiazolidines **26a–e** and thiazolidinones **27a,b**, respectively (Scheme 7B) [86]. Interestingly, the authors chose to assess in vitro AChE inhibition through a percentage increase in contraction of frog's Rectus abdominis, as opposed to the more common Ellman assay [60], making a direct comparison to other compounds described in this review difficult. Suffice it to say, all compounds showed AChE inhibitory activity that was comparable or better than tacrine except **25a**. In particular, **24b**, **26e**, and **27a,b** were all roughly at least twice as active as tacrine. COX-2 inhibition assays indicated that **24b**, **26e**, and **27a,b** showed IC₅₀ values between 0.76–0.89 μM, which was comparable to celecoxib (IC₅₀ = 0.84 μM). Of note, **26e** showed remarkable selectivity towards COX-2 over COX-1 (13-fold more potent towards COX-2, better than celecoxib), which is beneficial for reducing adverse renal and gastrointestinal side effects [88]. The hepatotoxicity was investigated through determination of serum glutamic pyruvic transaminase (SGPT) levels, and all compounds proved less hepatotoxic than tacrine. Molecular modeling with hAChE showed similar interactions for all compounds. For example, **27a,b** (Figure 6) was predicted to interact in the PAS with the tricyclic core showing favorable hydrophobic interactions with Tyr341, Tyr337, Phe338, and Val294. The 4-chlorophenyl substituent also showed hydrophobic interactions with Tyr341 and Trp286, and the quinolinyl nitrogen was predicted to H-bond with Arg296. The thiazolidinone moiety showed a favorable interaction with Glu292 and Ser293 [86].



Scheme 7. (A) Structure of pyrazolotacrines **24a–d**, **25a,b**, **26a–e**, and **27a,b** [86]. (B) Synthesis of pyrazolotacrines **24a–d**, **25a,b**, **26a–e**, and **27a,b**. Reagents and conditions: (i) R-CHO, piperidine, EtOH, Δ, 4 h, 80–90%; (ii) R₁-NCS, EtOH, Δ, 4–6 h, 83–89%; (iii) R₂-COCH₂Br, NaOAc, 1,4-dioxane, Δ, 4–6 h, 60–92%; (iv) ethyl bromoacetate, NaOAc, 1,4-dioxane, Δ, 4–6 h, 68–79%.

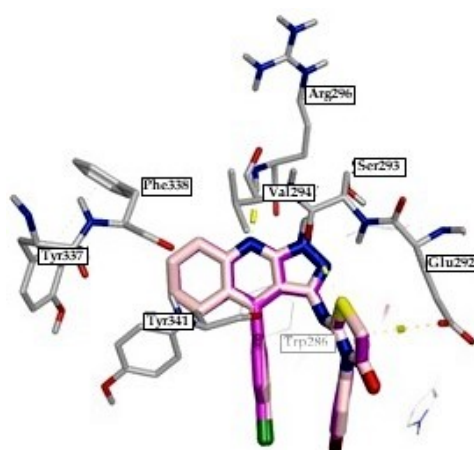


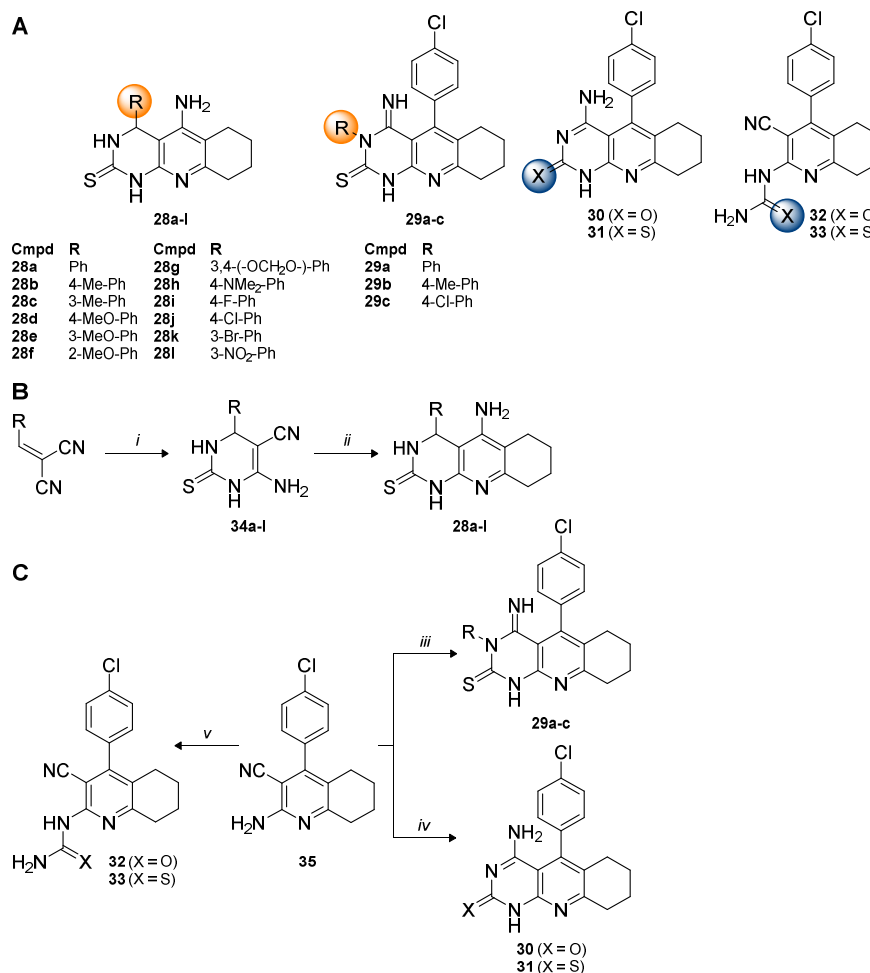
Figure 6. Molecular modeling of **27a** (rose) and **27b** (purple) with *hAChE* showing the interaction with the PAS (adapted from [86], with permission from Elsevier). Key interactions noted are the tricyclic core showing favorable hydrophobic interactions with Tyr341, Tyr337, Phe338, and Val294, the 4-chlorophenyl substituent showing hydrophobic interactions with Tyr341 and Trp286, the quinolinyl nitrogen showing an H-bond with Arg296, and the thiazolidinone moiety showing favorable interactions with Glu292 and Ser293.

8. Urea and Thiourea Tacrines

Still further replacement of the aromatic *A*-ring of tacrine with additional heterocycles has resulted in thiourea and urea tacrines (Scheme 8A) [89,90]. Thiourea tacrines **28a–l** were designed to combine tacrine and 3,4-dihydropyrimidin-2(1*H*)-thiones, known as calcium channel blockers [91,92] that have also shown metal-mediated, A β -related neuroprotection [93], into a multifunctional scaffold. The 3,4-dihydropyrimidin-2(1*H*)-thione moiety **34a–l** was prepared by the reaction of substituted arylidenemalononitriles with thiourea in the presence of NaOMe. The exocyclic nitrile and amine then readily underwent the Friedländer reaction with cyclohexanone in the presence of AlCl₃ to afford the target compounds as racemic mixtures (Scheme 8B) [89]. The synthesis of **29a–c** and **30–33** was done in one-step from the 2-amino-3-cyanotetrahydroquinoline **35**. Precursor **35** could be condensed with aryl isothiocyanates to afford cyclized thiourea tacrines **29a–c**, or it could be fused with urea or thiourea under high temperature (300 °C) to afford cyclized urea and thiourea tacrines **30** and **31** or moderate temperature (200 °C) to afford the open chain urea and thiourea tacrines **32** and **33** (Scheme 8C) [90].

Thiourea tacrines **28a–l** showed a promising biological profile. The most potent *hAChE* inhibitor was **28k** (IC₅₀ = 37.3 nM), which had a 3-bromophenyl substituent and was 10-fold more potent than tacrine (IC₅₀ = 374 nM). In addition, **28e**, which had a 3-methoxyphenyl substituent, was the next most potent but significantly weaker (IC₅₀ = 3.05 μ M). All other compounds in this series were significantly weaker AChEi (IC₅₀ > 5 μ M). Both **28e** and **28k** showed non-competitive inhibition by Lineweaver-Burk plot analysis, suggesting PAS interaction. This was confirmed by molecular modeling with *hAChE* where (*R*)-**28k** was predicted to bind to the PAS by π - π interactions with the phenyl ring and Trp286 and Tyr72 and the aminopyridine ring and Tyr341. H-bonds were also seen between the tacrine-like amine and Asp74, and the bromo substituent was involved in halogen bonds. Overall binding of the *S*-enantiomer was similar. Notably, **28e** was also predicted to bind to the PAS, but it lacked any binding contribution from the methoxy substituent, which may explain its reduced activity. In addition, compared to known calcium channel blocker nimodipine (49.62%), both **28e** and **28k** showed similar inhibition of Ca²⁺ influx (30.40% and 42.23%), but neither **28e** nor **28k** showed significant inhibition of A β ₁₋₄₂ self-induced aggregation. In addition, **28e** was particularly promising in that it displayed no hepatotoxicity to HepG2 cells at concentrations up to 300 μ M [89]. For **29a–c** and **30–33**, Ragab et al. chose to assess the *in vitro* AChE inhibition again through the less common percentage increase in contraction of frog's Rectus abdominis, making direct comparison to other compounds described in

this review difficult. However, it is still noted that all compounds showed promising AChE inhibitory activity except compound **29b**. Hepatotoxicity was investigated through the determination of SGPT levels and glutathione (GSH) levels, and all compounds proved less hepatotoxic than tacrine. In silico calculations predicted that all compounds had promising drug-like characteristics [90].

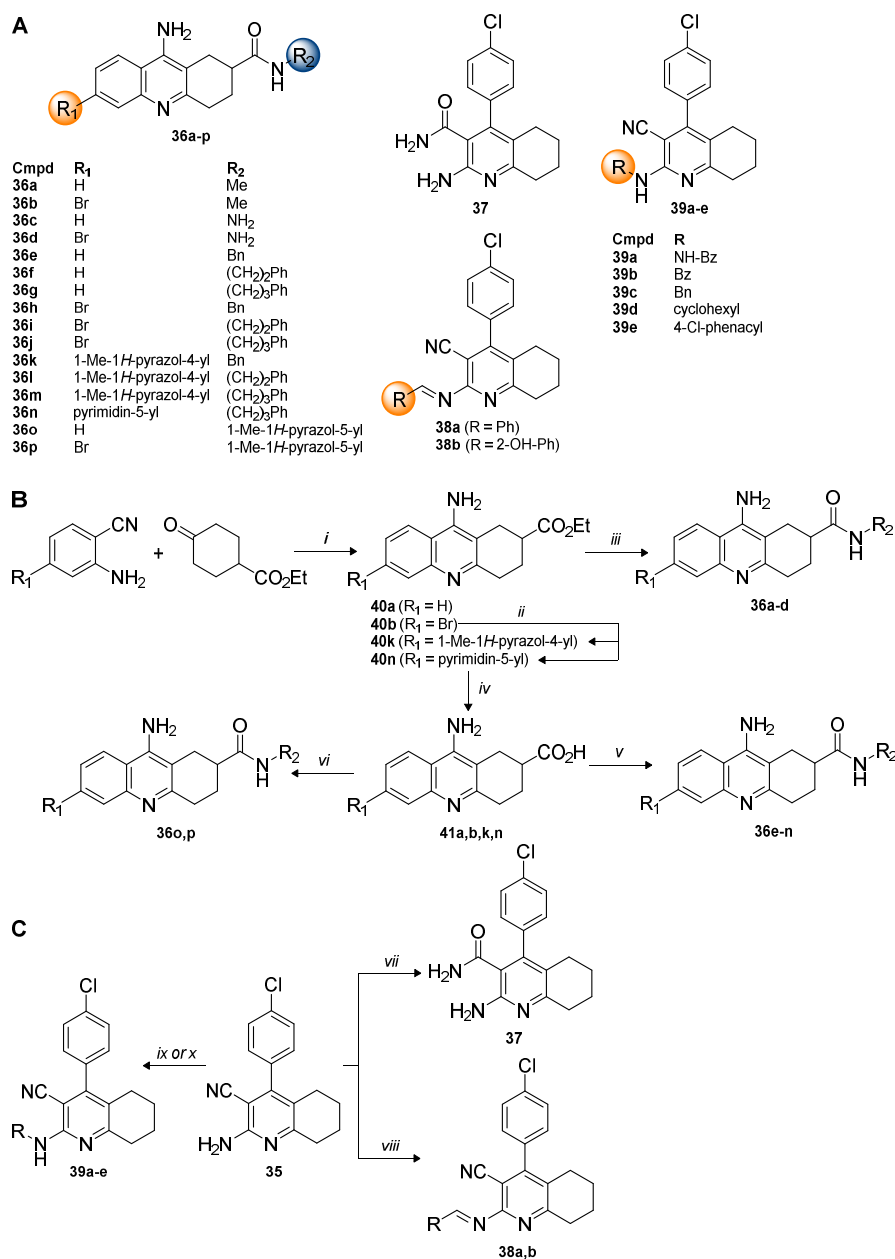


Scheme 8. (A) Structure of thiourea tacrines **28a–l**, **29a–c**, **31**, and **33** and urea tacrines **30** and **32** [89,90]. (B) Synthesis of thiourea tacrines **28a–l**. (C) Synthesis of thiourea and urea tacrines **29a–c** and **30–33**. Reagents and conditions: (i) Thiourea, NaOMe, EtOH, Δ , 12 h, 10–29%; (ii) cyclohexanone, AlCl₃, DCE, MWI, 1–2 h, 46–70%; (iii) SCN-R, pyridine, Δ , 10 h, 85–86%; (iv) urea or thiourea, 300 °C, 1 h, 64–74%; (v) urea or thiourea, 200 °C, 1 h, 76–83%.

9. Amido-, Amino-, and Iminotacrines

Amidotacrines **36a–p** were designed to explore the effect of adding an amide moiety to the 2-position of the cyclohexyl C-ring of tacrine, an underexplored SAR [94]. Meanwhile, amino- (**37** and **39a–e**) and iminotacrines **38a,b** focus on replacing the aromatic A-ring of tacrine with amine or imine moieties (Scheme 9A) [90]. Synthetically, amidotacrines were accessed via the key intermediate ethyl 2-tacrine carboxylate (**40a**) or the corresponding 6-bromo analog **40b**, which were prepared by the Friedländer reaction with 2-aminobenzonitriles, ethyl 4-oxocyclohexanecarboxylate, and BF₃·Et₂O (Scheme 9B). To investigate the effect of different heterocyclic substituents at the 6-position, **40b** was subjected to Pd-catalyzed Suzuki-Miyaura cross-coupling with the corresponding pyrazolo- or pyrimido-boronic ester to give **40k** and **40n**, respectively. Nucleophilic acyl substitution of **40a/b** with methylamine or hydrazine afforded **36a–d**. Alternatively, **40a,b,k,n** could be saponified to acids **41a,b,k,n** and coupled to various phenylalkylamines using T₃P to afford **36e–n** or coupled to

5-amino-1-methyl-1*H*-pyrazole using HATU to afford **36o,p** [94]. Compound **35**, for the synthesis of amino- and iminotacrine, could be hydrolyzed with 70% sulfuric acid to afford **37**, condensed with aryl aldehydes or benzoic acid hydrazide to afford Schiff bases **38a,b** or benzoylhydrazide **39a**, and acylated with benzoyl chloride or alkylated with different alkyl halides to afford derivatives **39b–e** (Scheme 9C) [90].



Scheme 9. (A) Structure of amido- (**36a–p**), amino- (**37** and **39a–e**), and iminotacrine **38a,b** [90,94]. (B) Synthesis of amidotacrine **36a–p**. (C) Synthesis of amino- (**37** and **39a–e**) and iminotacrine **38a,b**. Reagents and conditions: (i) $\text{BF}_3 \cdot \text{Et}_2\text{O}$, toluene, Δ , 4 h, 84%; (ii) 1-methylpyrazole-4-boronic acid pinacol ester or 5-pyrimidineboronic acid pinacol ester, Na_2CO_3 , $\text{Pd}(\text{PPh}_3)_4$, 1,4-dioxane/ H_2O , Δ , 2 h, 52%; (iii) NH_4OH or $\text{N}_2\text{H}_4 \cdot \text{H}_2\text{O}$, MeOH, 60 °C, 2–3 h, 73–85%; (iv) $\text{LiOH} \cdot \text{H}_2\text{O}$, THF/ H_2O /MeOH, rt, 3 h, 79–90%; (v) benzylamine or phenylethylamine or phenylpropylamine, T_3P , TEA, DMF, 60 °C, 4 h, 59–67%; (vi) 5-amino-1-methyl-1*H*-pyrazole, HATU, DIPEA, DMF, rt, 12 h, 63–71%; (vii) 70% H_2SO_4 , Δ , 5 h; (viii) $\text{R}-\text{C}_6\text{H}_4-\text{CHO}$, pyridine, Δ , 6 h, 87–90%; (ix) $\text{NH}_2\text{NH}-\text{Bz}$, Δ , 1 h, 84%; (x) $\text{X}-\text{R}$ (where $\text{X} = \text{Cl}$ or Br), 1,4-dioxane, Δ , 5–10 h, 69–89%.

With two exceptions, all amidotacrines **36a–p** were more potent than tacrine (*EeAChE* $IC_{50} = 94.69$ nM), and the best inhibitor was **36g** ($IC_{50} = 5.17$ nM), which had no substituent at the 6-position of the tacrine core and a phenylpropylamide at the 2-position (Table 4). SAR indicated that the phenylpropylamide at the 2-position gave the best inhibition of AChE, the bromo substituent at the 6-position seemed to have little effect, and a heterocycle (pyrazolo or pyrimido) at the 6-position decreased inhibition. Of note, **36c** with no substituent at the 6-position and the hydrazide at the 2-position was a potent inhibitor ($IC_{50} = 12.97$ nM). Molecular modeling with *TcAChE* showed that most compounds investigated positioned the tacrine moiety in the CAS, exhibiting π - π stacking with Trp84 and Tyr337 and H-bonding to His447, and oriented the 2-position towards the PAS allowing the amides to make key contacts with residues there. Of note, **36g** was positioned to allow the amide nitrogen to H-bond with Tyr124, and **36c** was positioned to allow the hydrazide to H-bond with Tyr337 (Figure 7). Compound **36c** was particularly promising as it uniquely, among the compounds tested, showed no cytotoxicity to HEK-293 cells or HepG2 cells at concentrations up to 300 μ M [94]. Amino- and iminotacrines **37**, **38a,b**, **39a–e**, also prepared by Ragab et al. and tested in an uncommon AChEi assay (see above), showed promising AChE inhibitory activity with the exception of compounds **39a,b**. Compound **39c**, with a 2-benzylamino substituent, had the highest activity (nearly 2-fold more active than tacrine). Molecular modeling of **39c** with *hAChE* showed H-bonding between the benzylamino NH and Asp93 and between the nitrogen of the CN group and Tyr96, as well as hydrophobic interactions with various amino acids. This compound also was less hepatotoxic than tacrine and predicted to have promising drug-like characteristics [90].

Table 4. Inhibition of *EeAChE* by amidotacrines **36a–p** (data from [94]).

Cmpd	IC_{50} (nM)	Potency Index ¹	Cmpd	IC_{50} (nM)	Potency Index ¹
36a	-	-	36i	24.10 \pm 3.43	3.93
36b	28.59 \pm 3.59	3.31	36j	7.14 \pm 0.78	13.3
36c	12.97 \pm 0.47	7.30	36k	191.11 \pm 10.69	0.50
36d	-	-	36l	188.70 \pm 27.72	0.50
36e	37.16 \pm 4.23	2.55	36m	57.64 \pm 9.94	1.64
36f	16.84 \pm 2.12	5.62	36n	40.78 \pm 5.43	2.32
36g	5.17 \pm 0.24	18.3	36o	-	-
36h	33.74 \pm 1.96	2.81	36p	17.72 \pm 1.51	5.34

¹ Compared to tacrine. Potency index = IC_{50} (nM) tacrine/ IC_{50} (nM) cmpd. The red places emphasis on compounds highlighted in the text.

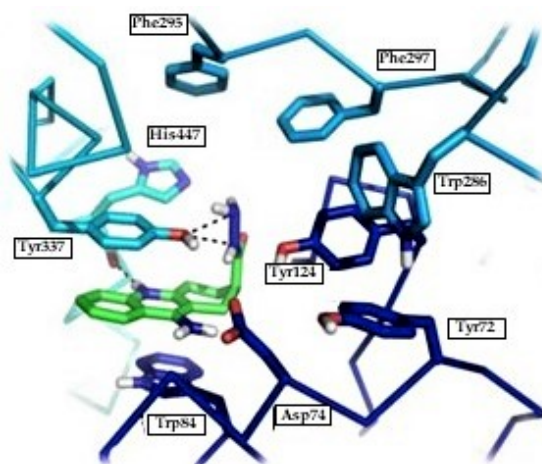


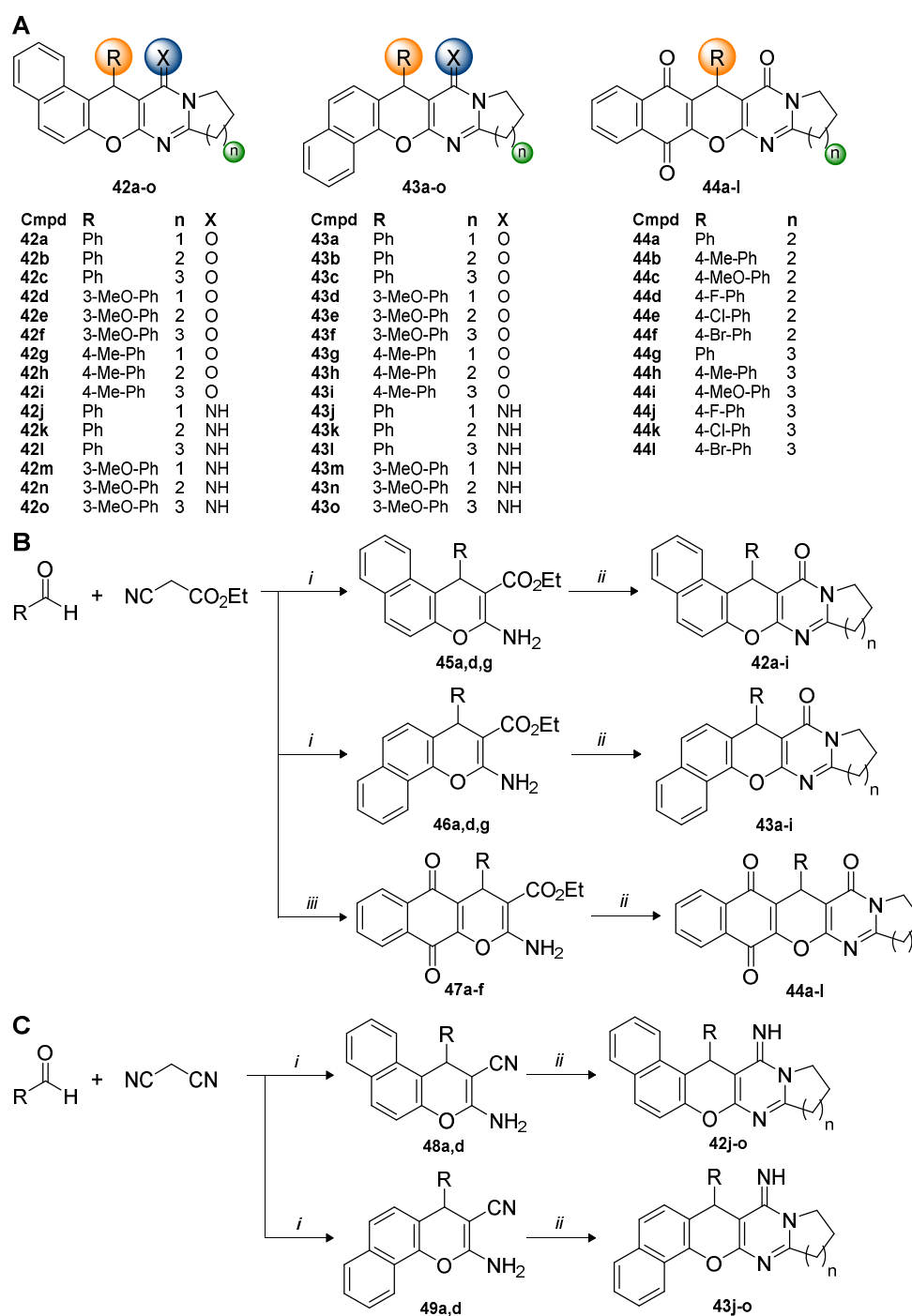
Figure 7. Molecular modeling of **36c** with *TcAChE* showing the interaction with the CAS (adapted from [94], with permission from Elsevier). Key interactions noted are the tacrine moiety π - π stacking with Trp84 and Tyr337 and H-bonding to His447 and the hydrazide H-bonding with Tyr337.

10. Naphthalene and Naphthoquinone Pyranopyrimidinones/Pyrimidinimines

Pyranopyrimidinones and pyranopyrimidinimines **42a–o**, **43a–o**, and **44a–l** (Scheme 10A) focus on two key modifications to the tacrine scaffold to modulate AChE inhibition and antioxidant activity: (1) Replacement of the aromatic *A*-ring with a fused pyranonaphthalene or pyranonaphthoquinone moiety and (2) change of the central aromatic *B*-ring from an aminopyridine to a pyrimidinone or pyrimidinimine [95–97]. Several examples of the former modification have been presented herein, but the latter remains underexplored. The transition to a pyrimidinone or pyrimidinimine is based on the fact that quinazolinone and quinazolinimine derivatives inspired by naturally occurring alkaloids structurally resemble tacrine (e.g., deoxyvasicinone) and have shown promising activity as AChEi [98–102]. The naphthalene pyranopyrimidinones **42a–i** and **43a–i** were prepared using a three-component, one-pot reaction with ethyl cyanoacetate, benzaldehydes, and 2- or 1-naphthol in the presence of piperidine to give **45a,d,g** and **46a,d,g**, followed by condensation with lactams in the presence of POCl₃ (Scheme 10B) [95]. Similarly, the pyranopyrimidinimines **42j–o** and **43j–o** were prepared using the same three-component, one-pot reaction with the exception of malononitrile in place of ethyl cyanoacetate to give **48a,d** and **49a,d**. Subsequent condensation with lactams in the presence of POCl₃ gave the desired compounds (Scheme 10C) [96]. Moreover, in a similar fashion, naphthoquinone pyranopyrimidinones **44a–l** were prepared using a three-component, one-pot reaction with ethyl cyanoacetate, benzaldehydes, and 2-hydroxynaphthalene-1,4-dione in the presence of potassium phthalimide-*N*-oxyl [103] to give **47a–f**. Condensation with lactams in the presence of POCl₃ as before gave the desired compounds (Scheme 10B) [97].

Among these three related series of compounds, a strong inhibition of AChE, such as tacrine, was generally maintained. For example, **42e**, containing a piperidine-fused ring, 3-methoxyphenyl substituent, and derived from 2-naphthol was the most potent of the naphthalene pyranopyrimidinones regarding *Ee*AChE inhibition (IC₅₀ = 30.5 nM) and was comparable to tacrine (IC₅₀ = 44.3 nM) (Table 5) [95]. In addition, **42n**, also containing a piperidine-fused ring, 3-methoxyphenyl substituent, and derived from 2-naphthol, was the most potent of the pyranopyrimidinimines (IC₅₀ = 3.2 nM), and this was followed closely by **42o** (IC₅₀ = 5.3 nM) bearing an azepane-fused ring (Table 5) [96]. Several of the naphthoquinone pyranopyrimidinones were similar in potency to tacrine (*Ee*AChE IC₅₀ = 31 nM). Of interest were the most potent **44f** (IC₅₀ = 44 nM), which contained a piperidine-fused ring and 4-bromophenyl substituent, and the similarly potent **44a** (IC₅₀ = 52 nM), which contained a piperidine-fused ring and phenyl substituent [97]. Notably, across all three series, even the worst inhibitor was still fairly potent (IC₅₀ ≈ 250–550 nM).

Compound **42e** displayed a mixed-type inhibition by the Lineweaver-Burk plot analysis. Additionally, it displayed potent antioxidant activity by the ORAC assay (4.7 Trolox equivalents) and showed no toxicity in HepG2 cells at concentrations up to 1 mM, but its BBB permeability is questionable (PAMPA-BBB, $P_e = 3.6 \times 10^{-6}$ cm/s) [95]. For the pyranopyrimidinimines, SAR clearly showed the 3-methoxyphenyl substituent to be more potent than the phenyl, and the 2-naphthol derived compounds to be more potent than those derived from 1-naphthol. Compound **42n** displayed noncompetitive inhibition by the Lineweaver-Burk plot analysis, which agrees with molecular modeling predicting binding of the *S*-enantiomer (but not *R*) of **42n** with the mid-gorge region of *h*AChE (Figure 8). Key interactions include a π - π stacking between Trp86 and the benzochromeno moiety and an H-bond between Asp74 and the imino moiety. Additionally, **42n** and **42o** displayed potent antioxidant activity by the ORAC assay (3.4 and 3.6 Trolox equivalents, respectively), but only **42o** showed a significant A β ₁₋₄₂ self-aggregation inhibition at 10 μ M (40.3%) [96]. All naphthoquinone pyranopyrimidinones displayed some degree of antioxidant activity by the ORAC assay (**44a** = 2.78 Trolox equivalents), but most displayed significant toxicity to HepG2 cells. In addition, **44a** was the exception as it maintained 84.5% HepG2 cell viability at 300 μ M and was 2-fold less toxic than tacrine at the same concentration [97].



Scheme 10. (A) Structure of naphthalene pyranopyrimidinones **42a–i** and **43a–i**, naphthoquinone pyranopyrimidinones **44a–l**, and naphthalene pyrimidinimines **42j–o** and **43j–o** [95–97]. (B) Synthesis of naphthalene pyranopyrimidinones **42a–i** and **43a–i** and naphthoquinone pyranopyrimidinones **44a–l**. (C) Synthesis of naphthalene pyranopyrimidinimines **42j–o** and **43j–o**. Reagents and conditions: (i) 2-Naphthol or 1-naphthol, piperidine, EtOH, MWI, 10 min, 68–95%; (ii) γ -butyrolactam or δ -valerolactam or ϵ -caprolactam, POCl₃, DCE or PhBr, MWI, 15 min, 70–96%; (iii) potassium phthalimide-*N*-oxyl, H₂O, Δ , 30–60 min, >90%.

Table 5. Inhibition of *Ee*AChE by naphthalene pyranopyrimidinones **42a–i** and **43a–i** and naphthalene pyrimidinimines **42j–o** and **43j–o** (data from [95,96]).

Cmpd	IC ₅₀ (nM)	Potency Index ¹	Cmpd	IC ₅₀ (nM)	Potency Index ¹
42a	518.4 ± 87.9	0.09	43a	317.8 ± 26.0	0.14
42b	55.5 ± 7.1	0.80	43b	383.5 ± 19.4	0.12
42c	300.8 ± 6.5	0.15	43c	290.5 ± 8.3	0.15
42d	60.7 ± 4.5	0.73	43d	326.7 ± 38.9	0.14
42e	30.5 ± 2.8	1.45	43e	153.2 ± 3.1	0.29
42f	107.5 ± 7.2	0.41	43f	195.3 ± 6.2	0.23
42g	111.9 ± 21.7	0.40	43g	115.8 ± 6.2	0.38
42h	55.9 ± 12.7	0.79	43h	193.4 ± 18.7	0.23
42i	166.6 ± 7.8	0.27	43i	173.8 ± 5.9	0.25
42j	67.8 ± 4.3	-	43j	379.5 ± 12.4	-
42k	9.9 ± 0.5	-	43k	93.5 ± 6.9	-
42l	34.0 ± 3.9	-	43l	96.1 ± 2.8	-
42m	6.0 ± 0.1	-	43m	44.9 ± 1.9	-
42n	3.2 ± 0.2	-	43n	12.1 ± 0.8	-
42o	5.3 ± 0.2	-	43o	52.6 ± 0.4	-

¹ Compared to tacrine. Potency index = IC₅₀ (nM) tacrine/IC₅₀ (nM) cmpd. The red places emphasis on compounds highlighted in the text.

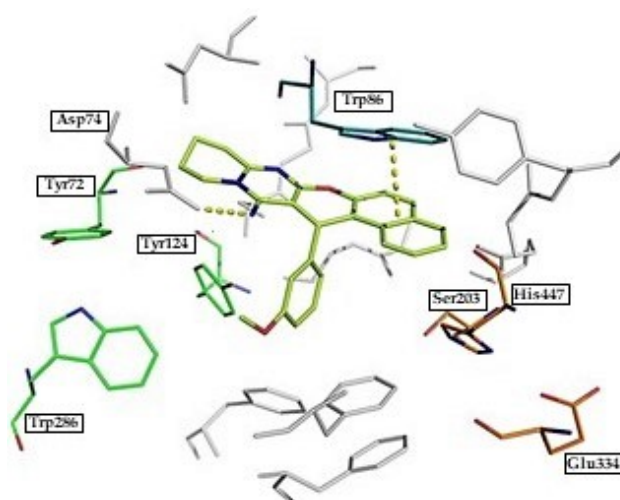
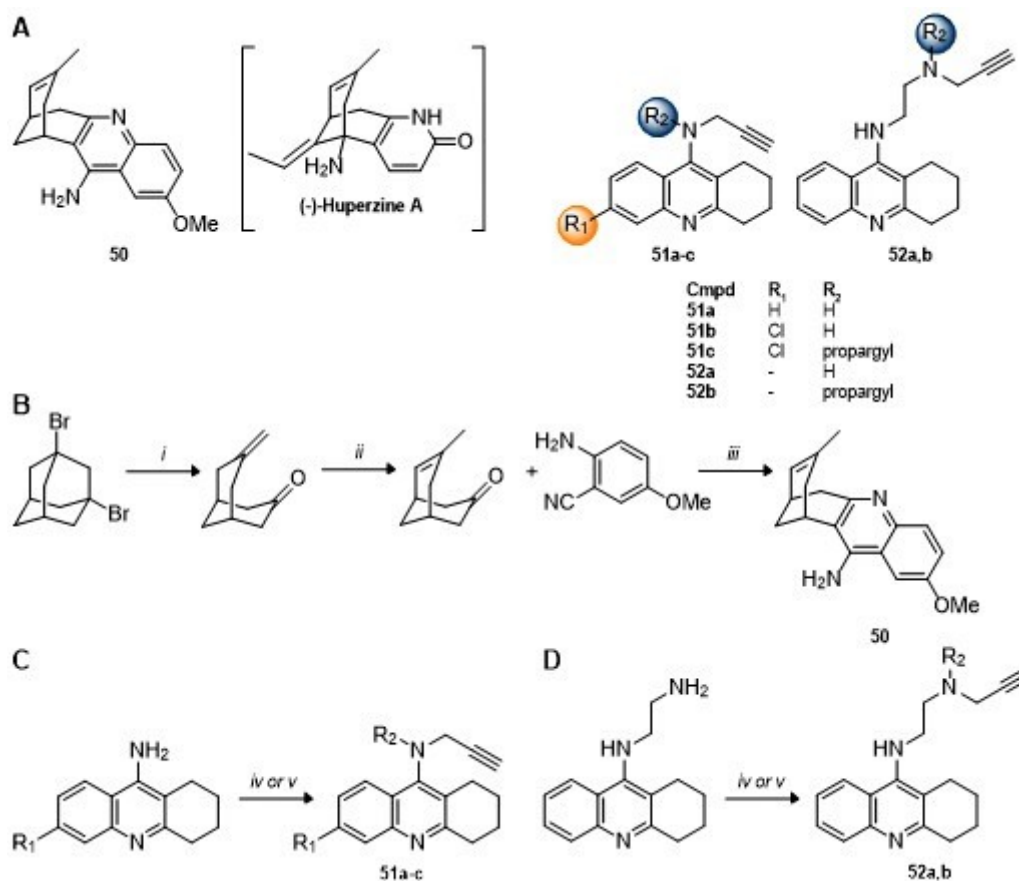


Figure 8. Molecular modeling of (*S*)-**42n** with *h*AChE showing the interaction with the mid-gorge region (adapted from [96], © 2016 WILEY-VCH Verlag GmbH & Co. KGaA, Weinheim). Key interactions noted are the π - π stacking between Trp86 and the benzochromeno moiety and an H-bond between Asp74 and the imino moiety.

11. Other Tacrines

This final section focuses on tacrine-based molecules with little structural similarity to those of previous sections. Huprines combine the aminoquinoline moiety of tacrine and the carbocyclic bridged moiety of huperine A (Scheme 11A), a naturally occurring sesquiterpene alkaloid AChEi. Of particular interest is huprine Y that has shown dramatic improvement compared to parent structures regarding AChE inhibition, while also showing neuroprotection against 3-nitropropionic acid-induced neurodegeneration in mice [104,105]. In constructing 2-methoxyhuprine (**50**) (Scheme 11A), Mezeiova et al. sought to maintain the beneficial properties of huprine Y while adding the reduced toxicity of 7-methoxytacrine by combining the carbocyclic bridged moiety and methoxyaminoquinoline moiety [106]. Synthetically, 1,3-dibromoadamantane was first fragmented to the ketone by reaction with NaOH at high temperature. Treatment with 5% Pd/C and H₂ in EtOH then led to isomerization of the carbon-carbon double bond. Finally, the Friedländer reaction with 2-amino-5-methoxybenzotrile

and AlCl_3 afforded racemic **50**, which was converted to the hydrochloride salt for biochemical testing (Scheme 11B). Regarding *hAChE* inhibition, 2-methoxyhuprine (**50**) showed a mixed-type inhibition, as determined by the Lineweaver-Burk analysis, with an $\text{IC}_{50} = 2.63 \mu\text{M}$ and was more nearly 4-fold more potent than the parent 7-methoxytacrine ($\text{IC}_{50} = 10 \mu\text{M}$). However, it was 8-fold less potent than tacrine ($\text{IC}_{50} = 320 \text{ nM}$) and 1600-fold less potent than the parent huprine Y ($\text{IC}_{50} = 1.64 \text{ nM}$). Interestingly, molecular modeling with *hAChE* predicted the more active enantiomer to be the *S,S*-enantiomer. In vitro assays predicted favorable CNS permeability (PAMPA-BBB, $P_e = 7.64 \times 10^{-6} \text{ cm/s}$) for **50**, but unfavorable toxicity, as in HepG2, ACHN, and SH-SY5Y cell lines, it showed significantly more toxicity than tacrine and 7-methoxytacrine (comparable to huprine Y) [106].

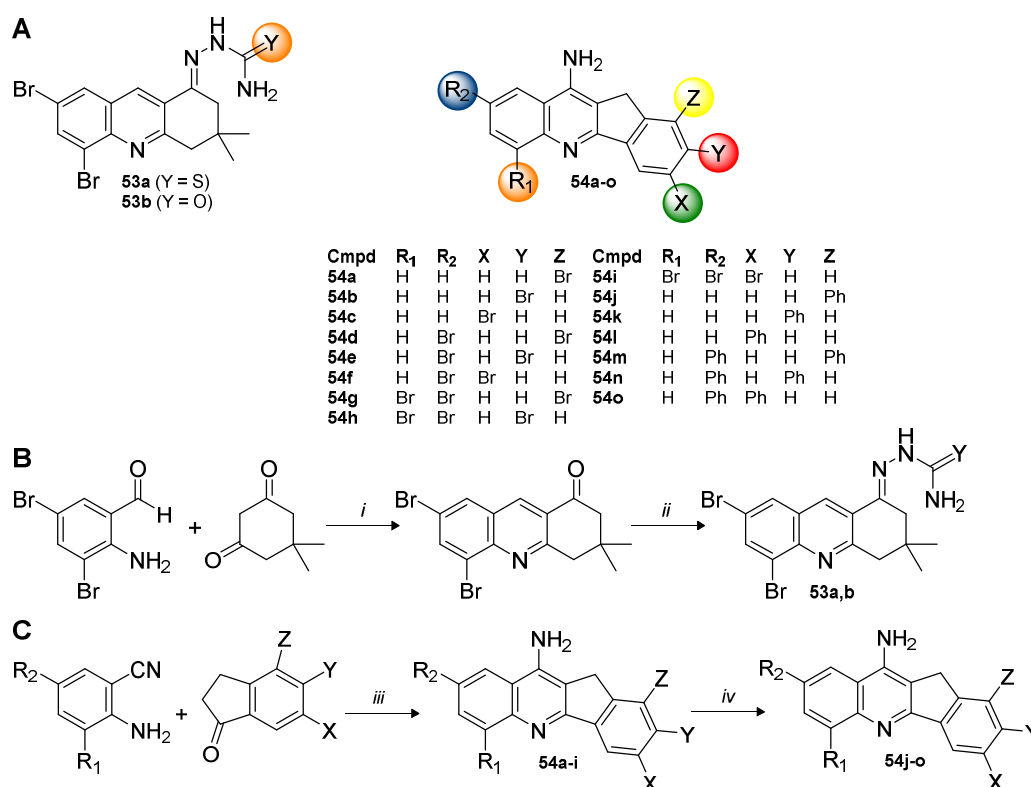


Scheme 11. (A) Structure of 2-methoxyhuprine (**50**) ((-)-huperzine A shown for reference) and propargyl tacrines **51a–c** and propargyl ethylenediamine tacrines **52a,b** [106,107]. (B) Synthesis of 2-methoxyhuprine (**50**). (C) Synthesis of propargyl tacrines **51a–c**. (D) Synthesis of propargyl ethylenediamine tacrines **52a,b**. Reagents and conditions: (i) 1 M NaOH, 1,4-dioxane, Δ , 18 h, 82%; (ii) 5% Pd/C, H_2 , EtOH, rt, 2 h, quant.; (iii) AlCl_3 , DCE, MWI, 2 h, 80%; (iv) propargyl bromide (1.1 eq), KOH or K_2CO_3 , MeCN, rt, 12–36 h, 35–82%; (v) propargyl bromide (2.1 eq), KOH or K_2CO_3 , MeCN, rt, 12–36 h, 35–82%.

Propargyl tacrines **51a–c** and propargyl ethylenediamine tacrines **52a,b** (Scheme 11A,C,D) were prepared by mono- or dialkylation of tacrine, 6-chlorotacrine, or ethylenediamine tacrine using propargyl bromide (1.1 or 2.1 eq.) [107]. A single propargyl group attached to tacrine or 6-chlorotacrine was found to increase *EeAChE* inhibition, as both **51a,b** were 2-fold more potent than the parent molecules ($\text{IC}_{50} = 51.3 \text{ nM}$ for **51a** vs. 104.8 nM for tacrine; 11.2 nM for **51b** vs. 23.5 nM for 6-chlorotacrine). Dipropargylation of tacrine or 6-chlorotacrine or mono- or dipropargylation of ethylenediamine tacrine was found to decrease inhibition. The Lineweaver-Burk plot indicated

a mixed-type inhibition for **51a**, and both **51a,b** showed decreased hepatotoxicity compared to tacrine [107].

Semicarbazone tacrines **53a,b** (Scheme 12A) were designed to incorporate semicarbazone or thiosemicarbazone at the 1-position of the tacrine tricyclic core [108]. These functional groups have diverse biological activity, and they have shown promise for AD as AChEi, metal chelators, and anti-A β compounds [109,110]. Condensation of 2-amino-3,5-dibromobenzaldehyde with dimedone afforded the tricyclic core, which readily condensed with thiosemicarbazide or semicarbazide in a second step to yield the target compounds **53a,b** (Scheme 12B). Inhibition studies showed that both were weak, mixed-type inhibitors of *EeAChE* (IC_{50} = 10.30 and 8.66 μ M, respectively) and were at least 200-fold less potent than tacrine (IC_{50} = 41.41 nM). Molecular modeling did predict a simultaneous CAS and PAS interaction with *EeAChE*, and in silico calculations also suggested favorable drug-like properties and lower toxicity than tacrine [108].



Scheme 12. (A) Structure of semicarbazone tacrines **53a,b** and indenoquinolines **54a–o** [108,111]. (B) Synthesis of semicarbazone tacrines **53a,b**. (C) Synthesis of indenoquinolines **54a–o**. Reagents and conditions: (i) 1,4-Dioxane, Δ , 24 h, 80%; (ii) thiosemicarbazide hydrochloride or semicarbazide hydrochloride, EtOH, Δ , 3 h, 75–79%; (iii) (a) $InCl_3$, toluene, Δ , 24 h; (b) 2 M NaOH, Δ , 24 h, 13–50%; (iv) $PhB(OH)_2$ (1.3 or 2.6 eq.), $Pd(PPh_3)_4$, K_2CO_3 , 1,4-dioxane, Δ , 4 h, 80–96%.

Lastly, Ekiz et al. prepared indenoquinoline tacrine analogs **54a–o** (Scheme 12A) for evaluation as AChEi and CAI [111]. $InCl_3$ -catalyzed Friedländer reaction of 2-aminobenzonitrile or brominated derivatives with bromoindanones gave **54a–i**. These were tested directly, or further derivatized to the mono- or diphenyl compounds **54j–o** by $Pd(PPh_3)_4$ -catalyzed Suzuki Coupling with phenylboronic acid (1.3 or 2.6 eq.) in the presence of aq. K_2CO_3 in dioxane (Scheme 12C). The monophenylindenoquinolines showed the most potent inhibition of *EeAChE* (IC_{50} = 37–57 nM), which was comparable to tacrine (IC_{50} = 59 nM), indicating that phenyl substituents at the 1-, 2-, or 3-positions were favorable (Table 6). The most potent was **54j** bearing a 1-phenyl substituent (IC_{50} = 37 nM). Additional SAR analysis showed that AChE inhibition was greatly reduced in the diphenylindenoquinolines and the mono-, di-, and tribromoindenoquinolines (IC_{50} > 1 μ M). The lone exception was the 1,8-dibromo compound

54d ($IC_{50} = 230$ nM). Compared to the known CAi, acetazolamide, all compounds showed a good inhibition activity against *hCAI* and *hCAII* ($IC_{50} < 1.3$ μ M), which may indicate additional therapeutic potential for these compounds [111].

Table 6. Inhibition of *EeAChE* by indenoquinolines **54a–o** (data from [111]).

Cmpd	IC_{50} (nM)	Potency Index ¹	Cmpd	IC_{50} (nM)	Potency Index ¹
54a	2610 ± 170	0.02	54i	3530 ± 117	0.02
54b	5700 ± 127	0.01	54j	37 ± 2.04	1.59
54c	2170 ± 273	0.03	54k	57 ± 2.39	1.04
54d	230 ± 15	0.26	54l	56 ± 2.49	1.05
54e	3730 ± 204	0.02	54m	4870 ± 102	0.01
54f	>10 μ M	-	54n	1090 ± 175	0.05
54g	5410 ± 1450	0.01	54o	-	-
54h	>10 μ M	-			

¹ Compared to tacrine. Potency index = IC_{50} (nM) tacrine/ IC_{50} (nM) cmpd. The red places emphasis on compounds highlighted in the text.

12. Conclusions

Many merged tacrine-based, multitarget-directed AChEi have been presented throughout this review. These compounds represent various chemical scaffolds, most commonly two of the three rings of tacrine's tricyclic core merged to other substituted heterocycles, that have been synthesized by diverse chemical methods. The Friedländer reaction has proven particularly important for building these tacrine-based inhibitors. SAR for AChE inhibition lacks a generalization across scaffolds and must be analyzed on a case-by-case basis. Nevertheless, some potent AChEi that have maintained or improved upon the already potent inhibition of tacrine have been identified, highlighted by **1s** ($IC_{50} = 58$ nM, 4.5-fold more potent than tacrine), **1x** ($IC_{50} = 44$ nM, 6-fold more potent than tacrine), **2u** ($IC_{50} = 34$ nM, 6-fold more potent than tacrine), **2x** ($IC_{50} = 81$ nM, 3-fold more potent than tacrine), **10l** ($IC_{50} = 40$ nM, similar potency to tacrine), **15i** ($IC_{50} = 69$ nM, 5-fold more potent than tacrine), **16l** ($IC_{50} = 10$ nM, 5.5-fold more potent than tacrine), **23l** ($IC_{50} = 49$ nM, 7.5-fold more potent than tacrine), **23o** ($IC_{50} = 23$ nM, 16-fold more potent than tacrine), **28k** ($IC_{50} = 37.3$ nM, 10-fold more potent than tacrine), **36c** ($IC_{50} = 12.97$ nM, 7-fold more potent than tacrine), **36g** ($IC_{50} = 5.17$ nM, 18-fold more potent than tacrine), **42o** ($IC_{50} = 5.3$ nM), **44a** ($IC_{50} = 52$ nM, similar potency to tacrine), and **54j** ($IC_{50} = 37$ nM, similar potency to tacrine).

A second group of compounds have been identified that either greatly reduced the hepatotoxicity of tacrine or showed significant secondary biological activity directed towards another aspect of AD (e.g., ROS, A β , metals), and this group is highlighted by **1f** (complete inhibition of A β_{1-40} *EeAChE*-induced aggregation, neuroprotection against oligomycin A/rotenone-induced oxidative stress in cortical neurons, and reduced hepatotoxicity), **2x** (moderate inhibitor of 15-LOX and reduced hepatotoxicity), **6d** (reduced hepatotoxicity, antioxidant capacity, and neuroprotection against oligomycin/rotenone and A β_{1-40} in SH-SY5Y cells), **11n** (ability to chelate Cu²⁺, Zn²⁺, and Fe²⁺), **15t** (high antioxidant capacity and low hepatotoxicity), **15ac** (inhibition of *EeAChE*-induced A β_{1-40} aggregation, reduced hepatotoxicity, and neuroprotection in SH-SY5Y cells against oxidative stress, A β_{1-40} aggregation, and tau-phosphorylation), **21** (reduced hepatotoxicity and neuroprotection in SH-SY5Y cells against ROS and tau hyperphosphorylation), **23l** (moderate ability to inhibit both self- and AChE-induced A β aggregation, reduced hepatotoxicity, and slight antioxidant activity), **26e** (selective COX-2 inhibition), **28k** (inhibition of Ca²⁺ influx), **42o** (antioxidant activity and significant A β_{1-42} self-aggregation inhibition), **44a** (antioxidant activity and reduced hepatotoxicity), and **54j** (inhibition of carbonic anhydrase). Altogether, compounds **2x**, **23l**, **28k**, **42o**, **44a**, and **54j** combine favorable AChE inhibition, favorable hepatotoxicity, and/or favorable secondary activity, and we feel they are the most promising for further study.

Going forward, we believe that continued research in this field is vital in the fight against AD. The most promising compounds identified should be further tested in animal models to evaluate if promising in vitro properties are maintained. The pharmacokinetic properties of the most promising compounds should also be further investigated. For example, the PAMPA-BBB data presented in initial screening results may be altered in an in vivo system, which would necessitate additional chemical modification to enhance pharmacokinetics. There is an additional chemical space that remains to be explored, and we envision additional heterocyclic fusions to the tacrine core to further explore SAR. As of yet, no “magic bullet” inhibitor has been identified. However, with each compound of this class that is synthesized and tested in combo, we gain incremental knowledge into the complex etiology and progression of AD that remains to be fully understood.

Author Contributions: Conceptualization, T.J.E.; investigation, T.J.E., D.L.M., and S.C.C.; writing—original draft preparation, T.J.E.; writing—review and editing, T.J.E., D.L.M., and S.C.C. All authors have read and agreed to the published version of the manuscript.

Funding: This research received no external funding.

Acknowledgments: We thank Michael Wilczanski for help in reviewing references. We thank the Penn State Behrend 2019–2020 Academic Year Undergraduate Research Grant that was partially used to support D.L.M. during work on this manuscript. Given the large volume of research and extended period devoted to the study of tacrine-based acetylcholinesterase inhibitors, we chose to focus this review only on compounds that have been first reported between January 2015–May 2020. We intend this review to be representative of the field but not necessarily all inclusive. We acknowledge those whose work in this field may have been omitted from discussion due to the scope of the manuscript.

Conflicts of Interest: The authors declare no conflict of interest.

Abbreviations

A β	Amyloid- β
ACh	Acetylcholine
AChE	Acetylcholinesterase
AChEi	Acetylcholinesterase inhibitor(s)
AD	Alzheimer’s disease
ADME	Absorption, distribution, metabolism, and excretion
APP	Amyloid precursor protein
BACE1	β -Secretase 1
BACE1i	β -Secretase 1 inhibitor(s)
BBB	Blood-brain barrier
CA	Carbonic anhydrase
CAi	Carbonic anhydrase inhibitor(s)
CAS	Catalytic active site
CNS	Central nervous system
COX-2	Cyclooxygenase 2
DABCO	1,4-Diazabicyclo[2.2.2]octane
DCE	Dichloroethane
DCM	Dichloromethane
DIPEA	<i>N,N</i> -Diisopropylethylamine
DMF	Dimethylformamide
DMSO	Dimethyl sulfoxide
<i>Ee</i>	<i>Electrophorus electricus</i>
GSH	Glutathione
<i>h</i>	Human
HATU	1-[Bis(dimethylamino)methylene]-1 <i>H</i> -1,2,3-triazolo[4,5- <i>b</i>]pyridinium 3-oxid hexafluorophosphate
IC ₅₀	Half maximal inhibitory concentration
KA	Kojic acid
15-LOX	15-Lipoxygenase

MOA	Monoamine oxidase
MOAi	Monoamine oxidase inhibitor(s)
MTDL	Multitarget-directed ligand
MWI	Microwave irradiation
NFTs	Neurofibrillary tangles
NMDAR	<i>N</i> -methyl- <i>D</i> -aspartate receptor
ORAC	Oxygen radical absorbance capacity
PAMPA	Parallel artificial membrane permeability assay
PAS	Peripheral anionic site
P_e	Effective permeability
ROS	Reactive oxygen species
SAR	Structure-activity relationship
SGPT	Serum glutamic pyruvic transaminase
<i>Tc</i>	<i>Torpedo californica</i>
TEA	Triethylamine
TFAA	Trifluoroacetic anhydride
THF	Tetrahydrofuran
T ₃ P	Propylphosphonic anhydride

References

- Silman, I.; Sussman, J.L. Acetylcholinesterase: ‘classical’ and ‘non-classical’ functions and pharmacology. *Curr. Opin. Pharmacol.* **2005**, *5*, 293–302. [[CrossRef](#)] [[PubMed](#)]
- Quinn, D.M. Acetylcholinesterase: Enzyme structure, reaction dynamics, and virtual transition states. *Chem. Rev.* **1987**, *87*, 955–979. [[CrossRef](#)]
- Ochoa, R.; Rodriguez, C.A.; Zuluaga, A.F. Perspectives for the structure-based design of acetylcholinesterase reactivators. *J. Mol. Graph. Model.* **2016**, *68*, 176–183. [[CrossRef](#)] [[PubMed](#)]
- Bajda, M.; Więckowska, A.; Hebda, M.; Guzior, N.; Sotriffer, C.A.; Malawska, B. Structure-based search for new inhibitors of cholinesterases. *Int. J. Mol. Sci.* **2013**, *14*, 5608–5632. [[CrossRef](#)] [[PubMed](#)]
- Mercey, G.; Verdelet, T.; Renou, J.; Kliachyna, M.; Baati, R.; Nachon, F.; Jean, L.; Renard, P.-Y. Reactivators of acetylcholinesterase inhibited by organophosphorus nerve agents. *Acc. Chem. Res.* **2012**, *45*, 756–766. [[CrossRef](#)] [[PubMed](#)]
- Silman, I.; Sussman, J.L. Acetylcholinesterase: How is structure related to function? *Chem. Biol. Interact.* **2008**, *175*, 3–10. [[CrossRef](#)]
- Dvir, H.; Silman, I.; Harel, M.; Rosenberry, T.L.; Sussman, J.L. Acetylcholinesterase: From 3D structure to function. *Chem. Biol. Interact.* **2010**, *187*, 10–22. [[CrossRef](#)]
- Rydberg, E.H.; Brumshtein, B.; Greenblatt, H.M.; Wong, D.M.; Shaya, D.; Williams, L.D.; Carlier, P.R.; Pang, Y.-P.; Silman, I.; Sussman, J.L. Complexes of alkylene-linked tacrine dimers with *Torpedo californica* acetylcholinesterase: Binding of bis(5)-tacrine produces a dramatic rearrangement in the active-site gorge. *J. Med. Chem.* **2006**, *49*, 5491–5500. [[CrossRef](#)]
- Radić, Z.; Manetsch, R.; Krasinski, A.; Raushel, J.; Yamauchi, J.; Garcia, C.; Kolb, H.; Sharpless, K.B.; Taylor, P. Molecular basis of interactions of cholinesterases with tight binding inhibitors. *Chem. Biol. Interact.* **2005**, *157*, 133–141. [[CrossRef](#)]
- 2020 Alzheimer’s disease facts and figures. *Alzheimer’s Dement.* **2020**, *16*, 391–460. [[CrossRef](#)]
- Drachman, D.A.; Leavitt, J. Human memory and the cholinergic system: A relationship to aging? *Arch. Neurol.* **1974**, *30*, 113–121. [[CrossRef](#)] [[PubMed](#)]
- Bartus, R.T. Evidence for a direct cholinergic involvement in the scopolamine-induced amnesia in monkeys: Effects of concurrent administration of physostigmine and methylphenidate with scopolamine. *Pharmacol. Biochem. Behav.* **1978**, *9*, 833–836. [[CrossRef](#)]
- Davies, P.; Maloney, A.J.F. Selective loss of central cholinergic neurons in Alzheimer’s disease. *Lancet* **1976**, *308*, 1403. [[CrossRef](#)]
- Perry, E.K.; Tomlinson, B.E.; Blessed, G.; Perry, R.H.; Cross, A.J.; Crow, T.T. Noradrenergic and cholinergic systems in senile dementia of Alzheimer type. *Lancet* **1981**, *318*, 149. [[CrossRef](#)]

15. Craig, L.A.; Hong, N.S.; McDonald, R.J. Revisiting the cholinergic hypothesis in the development of Alzheimer's disease. *Neurosci. Biobehav. Rev.* **2011**, *35*, 1397–1409. [[CrossRef](#)]
16. Pepeu, G.; Giovannini, M.G. Cholinesterase inhibitors and memory. *Chem. Biol. Interact.* **2010**, *187*, 403–408. [[CrossRef](#)]
17. Schliebs, R.; Arendt, T. The significance of the cholinergic system in the brain during aging and in Alzheimer's disease. *J. Neural Transm.* **2006**, *113*, 1625–1644. [[CrossRef](#)]
18. Oboudiyat, C.; Glazer, H.; Seifan, A.; Greer, C.; Isaacson, R.S. Alzheimer's disease. *Semin Neurol* **2013**, *33*, 313–329. [[CrossRef](#)]
19. Kreft, A.F.; Martone, R.; Porte, A. Recent advances in the identification of γ -secretase inhibitors to clinically test the A β oligomer hypothesis of Alzheimer's disease. *J. Med. Chem.* **2009**, *52*, 6169–6188. [[CrossRef](#)]
20. Kurz, A.; Perneckzy, R. Amyloid clearance as a treatment target against Alzheimer's disease. *J. Alzheimer's Dis.* **2011**, *24*, 61–73. [[CrossRef](#)]
21. Hardy, J.A.; Higgins, G.A. Alzheimer's disease: The amyloid cascade hypothesis. *Science* **1992**, *256*, 184. [[CrossRef](#)] [[PubMed](#)]
22. Jakob-Roetne, R.; Jacobsen, H. Alzheimer's disease: From pathology to therapeutic approaches. *Angew. Chem. Int. Ed.* **2009**, *48*, 3030–3059. [[CrossRef](#)] [[PubMed](#)]
23. Inestrosa, N.C.; Alvarez, A.; Pérez, C.A.; Moreno, R.D.; Vicente, M.; Linker, C.; Casanueva, O.I.; Soto, C.; Garrido, J. Acetylcholinesterase accelerates assembly of amyloid- β -peptides into Alzheimer's fibrils: Possible role of the peripheral site of the enzyme. *Neuron* **1996**, *16*, 881–891. [[CrossRef](#)]
24. De Ferrari, G.V.; Canales, M.A.; Shin, I.; Weiner, L.M.; Silman, I.; Inestrosa, N.C. A structural motif of acetylcholinesterase that promotes amyloid β -peptide fibril formation. *Biochemistry* **2001**, *40*, 10447–10457. [[CrossRef](#)]
25. Bartolini, M.; Bertucci, C.; Cavrini, V.; Andrisano, V. β -Amyloid aggregation induced by human acetylcholinesterase: Inhibition studies. *Biochem. Pharmacol.* **2003**, *65*, 407–416. [[CrossRef](#)]
26. Pithadia, A.S.; Lim, M.H. Metal-associated amyloid- β species in Alzheimer's disease. *Curr. Opin. Chem. Biol.* **2012**, *16*, 67–73. [[CrossRef](#)]
27. Savelieff, M.G.; Lee, S.; Liu, Y.; Lim, M.H. Untangling amyloid- β , tau, and metals in Alzheimer's disease. *Acc Chem. Biol.* **2013**, *8*, 856–865. [[CrossRef](#)]
28. Hureau, C. Coordination of redox active metal ions to the amyloid precursor protein and to amyloid- β peptides involved in Alzheimer disease. Part 1: An overview. *Coord. Chem. Rev.* **2012**, *256*, 2164–2174. [[CrossRef](#)]
29. Quintanilla, R.A.; Orellana, J.A.; Von Bernhardi, R. Understanding risk factors for Alzheimer's disease: Interplay of neuroinflammation, connexin-based communication and oxidative stress. *Arch. Med. Res.* **2012**, *43*, 632–644. [[CrossRef](#)]
30. McGeer, P.L.; McGeer, E.G. NSAIDs and Alzheimer disease: Epidemiological, animal model and clinical studies. *Neurobiol. Aging* **2007**, *28*, 639–647. [[CrossRef](#)]
31. Szekely, C.A.; Town, T.; Zandi, P.P. NSAIDs for the chemoprevention of Alzheimer's disease. In *Subcellular Biochemistry*; Springer: Dordrecht, The Netherlands, 2007; Volume 42, pp. 229–248.
32. Zündorf, G.; Reiser, G. Calcium dysregulation and homeostasis of neural calcium in the molecular mechanisms of neurodegenerative diseases provide multiple targets for neuroprotection. *Antioxid. Redox Signal.* **2010**, *14*, 1275–1288. [[CrossRef](#)] [[PubMed](#)]
33. Nimmrich, V.; Eckert, A. Calcium channel blockers and dementia. *Br. J. Pharmacol.* **2013**, *169*, 1203–1210. [[CrossRef](#)] [[PubMed](#)]
34. Praticò, D.; Zhukareva, V.; Yao, Y.; Uryu, K.; Funk, C.D.; Lawson, J.A.; Trojanowski, J.Q.; Lee, V.M.Y. 12/15-Lipoxygenase is increased in Alzheimer's disease: Possible involvement in brain oxidative stress. *Am. J. Pathol.* **2004**, *164*, 1655–1662. [[CrossRef](#)]
35. Joshi, Y.B.; Giannopoulos, P.F.; Praticò, D. The 12/15-lipoxygenase as an emerging therapeutic target for Alzheimer's disease. *Trends Pharmacol. Sci.* **2015**, *36*, 181–186. [[CrossRef](#)] [[PubMed](#)]
36. Schewe, T. 15-lipoxygenase-1: A prooxidant enzyme. *Biol. Chem.* **2002**, *383*, 365–374. [[CrossRef](#)]
37. Rubio-Perez, J.M.; Morillas-Ruiz, J.M. A review: Inflammatory process in Alzheimer's disease, role of cytokines. *Sci. World J.* **2012**, *2012*, 756357. [[CrossRef](#)]
38. Riederer, P.; Danielczyk, W.; Grünblatt, E. Monoamine oxidase-B inhibition in Alzheimer's disease. *NeuroToxicology* **2004**, *25*, 271–277. [[CrossRef](#)]

39. Pizzinat, N.; Copin, N.; Vindis, C.; Parini, A.; Cambon, C. Reactive oxygen species production by monoamine oxidases in intact cells. *Naunyn Schmiedeberg's Arch. Pharmacol.* **1999**, *359*, 428–431. [[CrossRef](#)]
40. Jang, B.G.; Yun, S.-M.; Ahn, K.; Song, J.H.; Jo, S.A.; Kim, Y.-Y.; Kim, D.K.; Park, M.H.; Han, C.; Koh, Y.H. Plasma carbonic anhydrase II protein is elevated in Alzheimer's disease. *J. Alzheimer's Dis.* **2010**, *21*, 939–945. [[CrossRef](#)]
41. Provensi, G.; Carta, F.; Nocentini, A.; Supuran, C.T.; Casamenti, F.; Passani, M.B.; Fossati, S. A new kid on the block? Carbonic anhydrases as possible new targets in Alzheimer's disease. *Int. J. Mol. Sci.* **2019**, *20*, 4724. [[CrossRef](#)]
42. Ittner, L.M.; Götz, J. Amyloid- β and tau—A toxic pas de deux in Alzheimer's disease. *Nat. Rev. Neurosci.* **2011**, *12*, 67–72. [[CrossRef](#)] [[PubMed](#)]
43. Swerdlow, R.H.; Burns, J.M.; Khan, S.M. The Alzheimer's disease mitochondrial cascade hypothesis: Progress and perspectives. *Biochim. Biophys. Acta* **2014**, *1842*, 1219–1231. [[CrossRef](#)] [[PubMed](#)]
44. Swerdlow, R.H.; Burns, J.M.; Khan, S.M. The Alzheimer's disease mitochondrial cascade hypothesis. *J. Alzheimer's Dis.* **2010**, *20*, S265–S279. [[CrossRef](#)] [[PubMed](#)]
45. Knapp, M.J.; Knopman, D.S.; Solomon, P.R.; Pendlebury, W.W.; Davis, C.S.; Gracon, S.I.; Apter, J.T.; Lazarus, C.N.; Baker, K.E.; Barnett, M.; et al. A 30-Week randomized controlled trial of high-dose tacrine in patients with Alzheimer's disease. *JAMA* **1994**, *271*, 985–991. [[CrossRef](#)]
46. Mehta, M.; Adem, A.; Sabbagh, M. New acetylcholinesterase inhibitors for Alzheimer's disease. *Int. J. Alzheimer Dis.* **2012**, *2012*, 728983. [[CrossRef](#)]
47. Ames, D.J.; Bhathal, P.S.; Davies, B.M.; Fraser, J.R.E. Hepatotoxicity of tetrahydroacridine. *Lancet* **1988**, *331*, 887. [[CrossRef](#)]
48. Pirmohamed, M.; Madden, S.; Park, B.K. Idiosyncratic drug reactions. *Clin. Pharmacokinet.* **1996**, *31*, 215–230. [[CrossRef](#)]
49. Youdim, M.B.H.; Buccafusco, J.J. Multi-functional drugs for various CNS targets in the treatment of neurodegenerative disorders. *Trends Pharmacol. Sci.* **2005**, *26*, 27–35. [[CrossRef](#)]
50. Youdim, M.B.H.; Buccafusco, J.J. CNS Targets for multi-functional drugs in the treatment of Alzheimer's and Parkinson's diseases. *J. Neural Transm.* **2005**, *112*, 519–537. [[CrossRef](#)]
51. Agatonovic-Kustrin, S.; Kettle, C.; Morton, D.W. A molecular approach in drug development for Alzheimer's disease. *Biomed. Pharmacother.* **2018**, *106*, 553–565. [[CrossRef](#)]
52. Pang, Y.-P.; Quiram, P.; Jelacic, T.; Hong, F.; Brimijoin, S. Highly potent, selective, and low cost bis-tetrahydroaminacrine inhibitors of acetylcholinesterase: Steps toward novel drugs for treating Alzheimer's disease. *J. Biol. Chem.* **1996**, *271*, 23646–23649. [[CrossRef](#)] [[PubMed](#)]
53. Bornstein, J.J.; Eckroat, T.J.; Houghton, J.L.; Jones, C.K.; Green, K.D.; Garneau-Tsodikova, S. Tacrine-mefenamic acid hybrids for inhibition of acetylcholinesterase. *MedChemComm* **2011**, *2*, 406–412. [[CrossRef](#)]
54. Kochi, A.; Eckroat, T.J.; Green, K.D.; Mayhoub, A.S.; Lim, M.H.; Garneau-Tsodikova, S. A novel hybrid of 6-chlorotacrine and metal-amyloid- β modulator for inhibition of acetylcholinesterase and metal-induced amyloid- β aggregation. *Chem. Sci.* **2013**, *4*, 4137–4145. [[CrossRef](#)]
55. Tsogoeva, S.B. Recent progress in the development of synthetic hybrids of natural or unnatural bioactive compounds for medicinal chemistry. *Mini Rev. Med. Chem* **2010**, *10*, 773–793. [[CrossRef](#)]
56. Colín-Lozano, B.; Estrada-Soto, S.; Chávez-Silva, F.; Gutiérrez-Hernández, A.; Cerón-Romero, L.; Giacomán-Martínez, A.; Almanza-Pérez, J.C.; Hernández-Núñez, E.; Wang, Z.; Xie, X.; et al. Design, synthesis and in combo antidiabetic bioevaluation of multitarget phenylpropanoic acids. *Molecules* **2018**, *23*, 340. [[CrossRef](#)]
57. Morphy, R.; Rankovic, Z. Designed multiple ligands. An emerging drug discovery paradigm. *J. Med. Chem.* **2005**, *48*, 6523–6543. [[CrossRef](#)]
58. Misik, J.; Nepovimova, E.; Pejchal, J.; Kassa, J.; Korabecny, J.; Soukup, O. Cholinesterase inhibitor 6-chlorotacrine—In vivo toxicological profile and behavioural effects. *Curr. Alzheimer Res.* **2018**, *15*, 552–560. [[CrossRef](#)]
59. Korabecny, J.; Musilek, K.; Holas, O.; Binder, J.; Zemek, F.; Marek, J.; Pohanka, M.; Opletalova, V.; Dohnal, V.; Kuca, K. Synthesis and in vitro evaluation of N-alkyl-7-methoxytacrine hydrochlorides as potential cholinesterase inhibitors in Alzheimer disease. *Bioorganic Med. Chem. Lett.* **2010**, *20*, 6093–6095. [[CrossRef](#)]
60. Ellman, G.L.; Courtney, K.D.; Andres, V., Jr.; Feather-Stone, R.M. A new and rapid colorimetric determination of acetylcholinesterase activity. *Biochem Pharm.* **1961**, *7*, 88–95. [[CrossRef](#)]
61. The UniProt, C. UniProt: A worldwide hub of protein knowledge. *Nucleic Acids Res.* **2018**, *47*, D506–D515. [[CrossRef](#)]

62. Navarrete-Vázquez, G.; Alaniz-Palacios, A.; Hidalgo-Figueroa, S.; González-Acevedo, C.; Ávila-Villarreal, G.; Estrada-Soto, S.; Webster, S.P.; Medina-Franco, J.L.; López-Vallejo, F.; Guerrero-Álvarez, J.; et al. Discovery, synthesis and in combo studies of a tetrazole analogue of clofibrilic acid as a potent hypoglycemic agent. *Bioorganic Med. Chem. Lett.* **2013**, *23*, 3244–3247. [[CrossRef](#)] [[PubMed](#)]
63. Khoobi, M.; Ghanoni, F.; Nadri, H.; Moradi, A.; Pirali Hamedani, M.; Homayouni Moghadam, F.; Emami, S.; Vosooghi, M.; Zadmard, R.; Foroumadi, A.; et al. New tetracyclic tacrine analogs containing pyrano[2,3-c]pyrazole: Efficient synthesis, biological assessment and docking simulation study. *Eur. J. Med. Chem.* **2015**, *89*, 296–303. [[CrossRef](#)] [[PubMed](#)]
64. Chioua, M.; Perez-Pena, J.; Garcia-Font, N.; Moraleda, I.; Iriepa, I.; Soriano, E.; Marco-Contelles, J.; Oset-Gasque, M.J. Pyranopyrazolotacrines as nonneurotoxic, Abeta-anti-aggregating and neuroprotective agents for Alzheimer's disease. *Future Med. Chem.* **2015**, *7*, 845–855. [[CrossRef](#)] [[PubMed](#)]
65. Derabli, C.; Boualia, I.; Abdelwahab, A.B.; Boulcina, R.; Bensouici, C.; Kirsch, G.; Debache, A. A cascade synthesis, in vitro cholinesterases inhibitory activity and docking studies of novel Tacrine-pyranopyrazole derivatives. *Bioorg Med. Chem. Lett* **2018**, *28*, 2481–2484. [[CrossRef](#)] [[PubMed](#)]
66. Pourabdi, L.; Khoobi, M.; Nadri, H.; Moradi, A.; Moghadam, F.H.; Emami, S.; Mojtahedi, M.M.; Haririan, I.; Forootanfar, H.; Ameri, A.; et al. Synthesis and structure-activity relationship study of tacrine-based pyrano[2,3-c]pyrazoles targeting AChE/BuChE and 15-LOX. *Eur J. Med. Chem.* **2016**, *123*, 298–308. [[CrossRef](#)]
67. Mahdavi, M.; Saeedi, M.; Gholamnia, L.; Jeddi, S.A.B.; Sabourian, R.; Shafiee, A.; Foroumadi, A.; Akbarzadeh, T. Synthesis of novel tacrine analogs as acetylcholinesterase inhibitors. *J. Heterocycl. Chem.* **2017**, *54*, 384–390. [[CrossRef](#)]
68. Hariri, R.; Afshar, Z.; Mahdavi, M.; Safavi, M.; Saeedi, M.; Najafi, Z.; Sabourian, R.; Karimpour-Razkenari, E.; Edraki, N.; Moghadam, F.H.; et al. Novel tacrine-based pyrano[3',4':5,6]pyrano[2,3-b]quinolinones: Synthesis and cholinesterase inhibitory activity. *Arch. Pharm. Weinh.* **2016**, *349*, 915–924. [[CrossRef](#)]
69. Dgachi, Y.; Martin, H.; Malek, R.; Jun, D.; Janockova, J.; Sepsova, V.; Soukup, O.; Iriepa, I.; Moraleda, I.; Maalej, E.; et al. Synthesis and biological assessment of KojoTacrines as new agents for Alzheimer's disease therapy. *J. Enzym. Inhib Med. Chem.* **2019**, *34*, 163–170. [[CrossRef](#)]
70. Gomes, A.J.; Lunardi, C.N.; Gonzalez, S.; Tedesco, A.C. The antioxidant action of Polypodium leucotomos extract and kojic acid: Reactions with reactive oxygen species. *Braz. J. Med. Biol. Res.* **2001**, *34*, 1487–1494. [[CrossRef](#)]
71. Boulebd, H.; Ismaili, L.; Bartolini, M.; Bouraiou, A.; Andrisano, V.; Martin, H.; Bonet, A.; Moraleda, I.; Iriepa, I.; Chioua, M.; et al. Imidazopyranotacrines as non-hepatotoxic, selective acetylcholinesterase inhibitors, and antioxidant agents for Alzheimer's disease therapy. *Molecules* **2016**, *21*, 400. [[CrossRef](#)]
72. Dgachi, Y.; Sokolov, O.; Luzet, V.; Godyn, J.; Panek, D.; Bonet, A.; Martin, H.; Iriepa, I.; Moraleda, I.; Garcia-Iriepa, C.; et al. Tetrahydropyranodiquinolin-8-amines as new, non hepatotoxic, antioxidant, and acetylcholinesterase inhibitors for Alzheimer's disease therapy. *Eur. J. Med. Chem.* **2017**, *126*, 576–589. [[CrossRef](#)] [[PubMed](#)]
73. Mahdavi, M.; Hariri, R.; Mirfazli, S.S.; Lotfian, H.; Rastergari, A.; Firuzi, O.; Edraki, N.; Larijani, B.; Akbarzadeh, T.; Saeedi, M. Synthesis and biological activity of some benzochromenoquinolinones: Tacrine analogs as potent anti-Alzheimer's agents. *Chem. Biodivers* **2019**, *16*, e1800488. [[CrossRef](#)] [[PubMed](#)]
74. Chioua, M.; Serrano, E.; Dgachi, Y.; Martin, H.; Jun, D.; Janockova, J.; Sepsova, V.; Soukup, O.; Moraleda, I.; Chabchoub, F.; et al. Synthesis, biological assessment and molecular modeling of racemic quinopyranotacrines for Alzheimer's disease therapy. *Chemistryselect* **2018**, *3*, 461–466. [[CrossRef](#)]
75. Wang, Z.; Li, W.; Wang, Y.; Li, X.; Huang, L.; Li, X. Design, synthesis and evaluation of clioquinol-ebiselen hybrids as multi-target-directed ligands against Alzheimer's disease. *Rsc. Adv.* **2016**, *6*, 7139–7158. [[CrossRef](#)]
76. Bermejo-Bescos, P.; Martin-Aragon, S.; Jimenez-Aliaga, K.L.; Ortega, A.; Molina, M.T.; Buxaderas, E.; Orellana, G.; Csaky, A.G. In vitro anti-amyloidogenic properties of 1,4-naphthoquinones. *Biochem. Biophys. Res. Commun.* **2010**, *400*, 169–174. [[CrossRef](#)]
77. Eghtedari, M.; Sarrafi, Y.; Nadri, H.; Mahdavi, M.; Moradi, A.; Homayouni Moghadam, F.; Emami, S.; Firoozpour, L.; Asadipour, A.; Sabzevari, O.; et al. New tacrine-derived AChE/BuChE inhibitors: Synthesis and biological evaluation of 5-amino-2-phenyl-4H-pyrano[2,3-b]quinoline-3-carboxylates. *Eur. J. Med. Chem.* **2017**, *128*, 237–246. [[CrossRef](#)]
78. Garcia-Font, N.; Hayour, H.; Belfaitah, A.; Pedraz, J.; Moraleda, I.; Iriepa, I.; Bouraiou, A.; Chioua, M.; Marco-Contelles, J.; Oset-Gasque, M.J. Potent anticholinesterasic and neuroprotective pyranotacrines as inhibitors of beta-amyloid aggregation, oxidative stress and tau-phosphorylation for Alzheimer's disease. *Eur. J. Med. Chem.* **2016**, *118*, 178–192. [[CrossRef](#)]

79. Ulus, R.; Zengin Kurt, B.; Gazioglu, I.; Kaya, M. Microwave assisted synthesis of novel hybrid tacrine-sulfonamide derivatives and investigation of their antioxidant and anticholinesterase activities. *Bioorg Chem.* **2017**, *70*, 245–255. [[CrossRef](#)]
80. Boulebd, H.; Ismaili, L.; Martin, H.; Bonet, A.; Chioua, M.; Marco Contelles, J.; Belfaitah, A. New (benz)imidazolopyridino tacrines as nonhepatotoxic, cholinesterase inhibitors for Alzheimer disease. *Future Med. Chem.* **2017**, *9*, 723–729. [[CrossRef](#)]
81. Benek, O.; Soukup, O.; Pasdiorova, M.; Hroch, L.; Sepsova, V.; Jost, P.; Hrabínova, M.; Jun, D.; Kuca, K.; Zala, D.; et al. Design, Synthesis and in vitro Evaluation of Indolotacrine Analogues as Multitarget-Directed Ligands for the Treatment of Alzheimer's Disease. *ChemMedChem* **2016**, *11*, 1264–1269. [[CrossRef](#)]
82. Ramos, E.; Palomino-Antolin, A.; Bartolini, M.; Iriepa, I.; Moraleda, I.; Diez-Iriepa, D.; Samadi, A.; Cortina, C.V.; Chioua, M.; Egea, J.; et al. Quinoxaline Tacrine QT78, a cholinesterase inhibitor as a potential ligand for Alzheimer's disease therapy. *Molecules* **2019**, *24*, 1503. [[CrossRef](#)]
83. Monge, A.; Palop, J.A.; Del Castillo, J.C.; Caldero, J.M.; Roca, J.; Romero, G.; Del Rio, J.; Lasheras, B. Novel antagonists of 5-HT₃ receptors. Synthesis and biological evaluation of piperazinylquinoxaline derivatives. *J. Med. Chem.* **1993**, *36*, 2745–2750. [[CrossRef](#)] [[PubMed](#)]
84. Alshareef, H.F.; Mohamed, H.; Salaheldin, A.M. Synthesis and biological evaluation of new tacrine analogues under microwave irradiation. *Chem. Pharm. Bull.* **2017**, *65*, 732–738. [[CrossRef](#)] [[PubMed](#)]
85. Jalili-Baleh, L.; Nadri, H.; Moradi, A.; Bukhari, S.N.A.; Shakibaie, M.; Jafari, M.; Golshani, M.; Homayouni Moghadam, F.; Firoozpour, L.; Asadipour, A.; et al. New racemic annulated pyrazolo[1,2-b]phthalazines as tacrine-like AChE inhibitors with potential use in Alzheimer's disease. *Eur. J. Med. Chem.* **2017**, *139*, 280–289. [[CrossRef](#)] [[PubMed](#)]
86. Mroueh, M.; Faour, W.H.; Shebaby, W.N.; Daher, C.F.; Ibrahim, T.M.; Ragab, H.M. Synthesis, biological evaluation and modeling of hybrids from tetrahydro-1H-pyrazolo[3,4-b]quinolines as dual cholinesterase and COX-2 inhibitors. *Bioorg Chem.* **2020**, *100*, 103895. [[CrossRef](#)]
87. Ragab, H.M.; Ashour, H.M.A.; Galal, A.; Ghoneim, A.I.; Haidar, H.R. Synthesis and biological evaluation of some tacrine analogs: Study of the effect of the chloro substituent on the acetylcholinesterase inhibitory activity. *Mon. Fitr Chem. Mon.* **2016**, *147*, 539–552. [[CrossRef](#)]
88. Patrono, C.; Rocca, B. Nonsteroidal antiinflammatory drugs: Past, present and future. *Pharmacol. Res.* **2009**, *59*, 285–289. [[CrossRef](#)]
89. Chioua, M.; Buzzi, E.; Moraleda, I.; Iriepa, I.; Maj, M.; Wnorowski, A.; Giovannini, C.; Tramarin, A.; Portali, F.; Ismaili, L.; et al. Tacripyrimidines, the first tacrine-dihydropyrimidine hybrids, as multi-target-directed ligands for Alzheimer's disease. *Eur. J. Med. Chem.* **2018**, *155*, 839–846. [[CrossRef](#)]
90. Ragab, H.M.; Teleb, M.; Haidar, H.R.; Gouda, N. Chlorinated tacrine analogs: Design, synthesis and biological evaluation of their anti-cholinesterase activity as potential treatment for Alzheimer's disease. *Bioorg Chem.* **2019**, *86*, 557–568. [[CrossRef](#)]
91. Atwal, K.S.; Swanson, B.N.; Unger, S.E.; Floyd, D.M.; Moreland, S.; Hedberg, A.; O'Reilly, B.C. Dihydropyrimidine calcium channel blockers. 3. 3-Carbamoyl-4-aryl-1,2,3,4-tetrahydro-6-methyl-5-pyrimidinecarboxylic acid esters as orally effective antihypertensive agents. *J. Med. Chem.* **1991**, *34*, 806–811. [[CrossRef](#)]
92. Zorkun, I.S.; Saraç, S.; Çelebi, S.; Erol, K. Synthesis of 4-aryl-3,4-dihydropyrimidin-2(1H)-thione derivatives as potential calcium channel blockers. *Bioorganic Med. Chem.* **2006**, *14*, 8582–8589. [[CrossRef](#)] [[PubMed](#)]
93. Tardiff, D.F.; Brown, L.E.; Yan, X.; Trilles, R.; Jui, N.T.; Barrasa, M.I.; Caldwell, K.A.; Caldwell, G.A.; Schaus, S.E.; Lindquist, S. Dihydropyrimidine-thiones and clioquinol synergize to target β -amyloid cellular pathologies through a metal-dependent mechanism. *ACS Chem. Neurosci.* **2017**, *8*, 2039–2055. [[CrossRef](#)] [[PubMed](#)]
94. Reddy, E.K.; Remya, C.; Mantosh, K.; Sajith, A.M.; Omkumar, R.V.; Sadasivan, C.; Anwar, S. Novel tacrine derivatives exhibiting improved acetylcholinesterase inhibition: Design, synthesis and biological evaluation. *Eur. J. Med. Chem.* **2017**, *139*, 367–377. [[CrossRef](#)] [[PubMed](#)]
95. Dgachi, Y.; Bautista-Aguilera, O.M.; Bencheikroun, M.; Martin, H.; Bonet, A.; Knez, D.; Godyn, J.; Malawska, B.; Gobec, S.; Chioua, M.; et al. Synthesis and biological evaluation of benzochromenopyrimidinones as cholinesterase inhibitors and potent antioxidant, non-hepatotoxic agents for Alzheimer's disease. *Molecules* **2016**, *21*, 634. [[CrossRef](#)]

96. Dgachi, Y.; Ismaili, L.; Knez, D.; Benchekroun, M.; Martin, H.; Szalaj, N.; Wehle, S.; Bautista-Aguilera, O.M.; Luzet, V.; Bonnet, A.; et al. Synthesis and biological assessment of racemic benzochromenopyrimidinimines as antioxidant, cholinesterase, and Abeta1-42 aggregation inhibitors for Alzheimer's disease therapy. *ChemMedChem* **2016**, *11*, 1318–1327. [[CrossRef](#)]
97. Dgachi, Y.; Martin, H.; Bonnet, A.; Chioua, M.; Iriepa, I.; Moraleda, I.; Chabchoub, F.; Marco-Contelles, J.; Ismaili, L. Synthesis and biological assessment of racemic benzochromenopyrimidinetriones as promising agents for Alzheimer's disease therapy. *Future Med. Chem.* **2017**, *9*, 715–721. [[CrossRef](#)]
98. Decker, M. Novel inhibitors of acetyl- and butyrylcholinesterase derived from the alkaloids dehydroevodiamine and rutaecarpine. *Eur. J. Med. Chem.* **2005**, *40*, 305–313. [[CrossRef](#)]
99. Huang, G.; Kling, B.; Darras, F.H.; Heilmann, J.; Decker, M. Identification of a neuroprotective and selective butyrylcholinesterase inhibitor derived from the natural alkaloid evodiamine. *Eur. J. Med. Chem.* **2014**, *81*, 15–21. [[CrossRef](#)]
100. Darras, F.H.; Wehle, S.; Huang, G.; Sotriffer, C.A.; Decker, M. Amine substitution of quinazolinones leads to selective nanomolar AChE inhibitors with 'inverted' binding mode. *Bioorg. Med. Chem.* **2014**, *22*, 4867–4881. [[CrossRef](#)]
101. Decker, M. Homobivalent quinazolinimines as novel nanomolar inhibitors of cholinesterases with dirigible selectivity toward butyrylcholinesterase. *J. Med. Chem.* **2006**, *49*, 5411–5413. [[CrossRef](#)]
102. Decker, M.; Krauth, F.; Lehmann, J. Novel tricyclic quinazolinimines and related tetracyclic nitrogen bridgehead compounds as cholinesterase inhibitors with selectivity towards butyrylcholinesterase. *Bioorg. Med. Chem.* **2006**, *14*, 1966–1977. [[CrossRef](#)] [[PubMed](#)]
103. Dekamin, M.G.; Eslami, M.; Maleki, A. Potassium phthalimide-N-oxyl: A novel, efficient, and simple organocatalyst for the one-pot three-component synthesis of various 2-amino-4H-chromene derivatives in water. *Tetrahedron* **2013**, *69*, 1074–1085. [[CrossRef](#)]
104. Muñoz-Torrero, D.; Camps, P. Huprines for Alzheimer's disease drug development. *Expert Opin. Drug Discov.* **2008**, *3*, 65–81. [[CrossRef](#)] [[PubMed](#)]
105. Canudas, A.M.; Pubill, D.; Sureda, F.X.; Verdaguer, E.; Camps, P.; Muñoz-Torrero, D.; Jiménez, A.; Camins, A.; Pallàs, M. Neuroprotective effects of (\pm)-huprine Y on in vitro and in vivo models of excitotoxicity damage. *Exp. Neurol.* **2003**, *180*, 123–130. [[CrossRef](#)]
106. Mezeiova, E.; Korabecny, J.; Sepsova, V.; Hrabínova, M.; Jost, P.; Muckova, L.; Kucera, T.; Dolezal, R.; Misik, J.; Spilovska, K.; et al. Development of 2-methoxyhuprine as novel lead for Alzheimer's disease therapy. *Molecules* **2017**, *22*, 1265. [[CrossRef](#)]
107. Mao, F.; Li, J.; Wei, H.; Huang, L.; Li, X. Tacrine-propargylamine derivatives with improved acetylcholinesterase inhibitory activity and lower hepatotoxicity as a potential lead compound for the treatment of Alzheimer's disease. *J. Enzym. Inhib. Med. Chem.* **2015**, *30*, 995–1001. [[CrossRef](#)]
108. Neto, D.C.F.; Lima, J.A.; De Almeida, J.S.F.D.; Franca, T.C.C.; do Nascimento, C.J.; Villar, J.D.F. New semicarbazones as gorge-spanning ligands of acetylcholinesterase and potential new drugs against Alzheimer's disease: Synthesis, molecular modeling, NMR, and biological evaluation. *J. Biomol. Struct. Dyn.* **2018**, *36*, 4099–4113. [[CrossRef](#)]
109. Lambert, C.; Beraldo, H.; Lievre, N.; Garnier-Suillerot, A.; Dorlet, P.; Salerno, M. Bis(thiosemicarbazone) copper complexes: Mechanism of intracellular accumulation. *J. Biol. Inorg. Chem.* **2013**, *18*, 59–69. [[CrossRef](#)]
110. Sinha, S.K.; Shrivastava, S.K. Synthesis, evaluation and molecular dynamics study of some new 4-aminopyridine semicarbazones as an anti-amnesic and cognition enhancing agents. *Bioorg. Med. Chem.* **2013**, *21*, 5451–5460. [[CrossRef](#)]
111. Ekiz, M.; Tutar, A.; Okten, S.; Butun, B.; Kocyigit, U.M.; Taslimi, P.; Topcu, G. Synthesis, characterization, and SAR of arylated indenoquinoline-based cholinesterase and carbonic anhydrase inhibitors. *Arch. Pharm. Wein.* **2018**, *351*, e1800167. [[CrossRef](#)]

